



HAL
open science

Enteric delivery of regenerating family member 3 alpha alters the intestinal microbiota and controls inflammation in mice with colitis

Marion Darnaud, Alexandre dos Santos, Patrick Gonzalez, Sandrine Augui, Claire Lacoste, Christophe Desterke, Gert de Hertogh, Emma Valentino, Emilie Braun, Jinzi Zheng, et al.

► To cite this version:

Marion Darnaud, Alexandre dos Santos, Patrick Gonzalez, Sandrine Augui, Claire Lacoste, et al.. Enteric delivery of regenerating family member 3 alpha alters the intestinal microbiota and controls inflammation in mice with colitis. *Gastroenterology*, 2018, 154 (4), pp.1009 -1037. 10.1053/j.gastro.2017.11.003 . hal-02626272

HAL Id: hal-02626272

<https://hal.inrae.fr/hal-02626272>

Submitted on 12 Jul 2021

HAL is a multi-disciplinary open access archive for the deposit and dissemination of scientific research documents, whether they are published or not. The documents may come from teaching and research institutions in France or abroad, or from public or private research centers.

L'archive ouverte pluridisciplinaire **HAL**, est destinée au dépôt et à la diffusion de documents scientifiques de niveau recherche, publiés ou non, émanant des établissements d'enseignement et de recherche français ou étrangers, des laboratoires publics ou privés.



Distributed under a Creative Commons Attribution - NonCommercial - NoDerivatives 4.0 International License

BASIC AND TRANSLATIONAL—ALIMENTARY TRACT

Enteric Delivery of Regenerating Family Member 3 alpha Alters the Intestinal Microbiota and Controls Inflammation in Mice With Colitis



Marion Darnaud,^{1,2,*} Alexandre Dos Santos,^{1,2,*} Patrick Gonzalez,^{1,2,*} Sandrine Augui,^{1,2} Claire Lacoste,^{1,2} Christophe Desterke,² Gert De Hertogh,³ Emma Valentino,^{1,2} Emilie Braun,^{1,2} Jinzi Zheng,^{4,5} Raphael Boisgard,^{4,5} Christel Neut,⁶ Laurent Dubuquoy,⁶ Franck Chiappini,^{1,2} Didier Samuel,^{1,2} Patricia Lepage,⁷ Francesca Guerrieri,⁸ Joel Doré,⁷ Christian Bréchet,^{1,2,9} Nicolas Moniaux,^{1,2} and Jamila Faivre^{1,2,10}

¹INSERM, U1193, Paul-Brousse University Hospital, Hepatobiliary Centre, Villejuif, France; ²University Paris-Sud, Université Paris-Saclay, Faculté de Médecine Le Kremlin-Bicêtre, France; ³Department of Imaging and Pathology, Unit of Translational Cell and Tissue Research, University of Leuven, Leuven, Belgium; ⁴CEA, DSV, Institut d'Imagerie Biomédicale, Orsay, France; ⁵INSERM, U1023, Université Paris-Sud, Orsay, France; ⁶LIRIC-U995, University Lille, Inserm, CHU Lille, Lille, France; ⁷Institut National de la Recherche Agronomique, UMR 1319 MICALIS, Jouy-en-Josas, France; ⁸Center for Life NanoScience@Sapienza, Istituto Italiano di Tecnologia, Roma, Italy; ⁹Pasteur Institute, Paris, France; and ¹⁰Assistance Publique-Hôpitaux de Paris (AP-HP), Pôle de Biologie Médicale, Paul-Brousse University Hospital, Villejuif, France

BACKGROUND & AIMS: Paneth cell dysfunction causes deficiencies in intestinal C-type lectins and antimicrobial peptides, which leads to dysbiosis of the intestinal microbiota, alters the mucosal barrier, and promotes development of inflammatory bowel diseases. We investigated whether transgenic (TG) expression of the human regenerating family member 3 alpha gene (*REG3A*) alters the fecal microbiota and affects development of colitis in mice. **METHODS:** We performed studies with C57BL/6 mice that express human regenerating family member 3 alpha (hREG3A) in hepatocytes, via the albumin gene promoter. In these mice, hREG3A travels via the bile to the intestinal lumen. Some mice were given dextran sodium sulfate (DSS) to induce colitis. Feces were collected from mice and the composition of the microbiota was analyzed by 16S ribosomal RNA sequencing. The fecal microbiome was also analyzed from mice that express only 1 copy of human *REG3A* transgene but were fed feces from control mice (not expressing hREG3A) as newborns. Mice expressing hREG3A were monitored for DSS-induced colitis after co-housing or feeding feces from control mice. Colitis was induced in another set of control and hREG3A-TG mice by administration of trinitrobenzene sulfonic acid; some mice were given intrarectal injections of the hREG3A protein. Colon tissues were collected from mice and analyzed by histology and immunohistochemistry to detect mucin 2, as well as by 16S ribosomal RNA fluorescence in situ hybridization, transcriptional analyses, and quantitative polymerase chain reaction. We measured levels of reactive oxygen species (ROS) in bacterial cultures and fecal microbiota using 2',7'-dichlorofluorescein diacetate and flow cytometry. **RESULTS:** The fecal microbiota of mice that express hREG3A had a significant shift in composition, compared with control mice, with enrichment of Clostridiales (Ruminococcaceae, Lachnospiraceae) and depletion of Bacteroidetes (Prevotellaceae); the TG mice

developed less-severe colitis following administration of DSS than control mice, associated with preserved gut barrier integrity and reduced bacterial translocation, epithelial inflammation, and oxidative damage. A similar shift in the composition of the fecal microbiota occurred after a few months in TG mice heterozygous for *REG3A* that harbored a wild-type maternal microbiota at birth; these mice developed less-severe forms of colitis following DSS administration. Cohoused and germ-free mice fed feces from *REG3A*-TG mice and given DSS developed less-severe forms of colitis and had reduced lipopolysaccharide activation of the toll-like receptor 4 and increased survival times compared with mice not fed feces from *REG3A*-TG mice. *REG3A* TG mice developed only mild colonic inflammation after exposure to 2,4,6-trinitrobenzene sulfonic acid, compared with control mice. Control mice given intrarectal hREG3A and exposed to 2,4,6-trinitrobenzene sulfonic acid showed less colon damage and inflammation than mice not given intrarectal hREG3A. Fecal samples from *REG3A*-TG mice had lower levels of ROS than feces from control mice during DSS administration. Addition of hREG3A to bacterial cultures reduced levels of ROS and increased survival of oxygen-sensitive commensal bacteria (*Faecalibacterium prausnitzii* and *Roseburia intestinalis*). **CONCLUSIONS:** Mice with hepatocytes that express hREG3A, which travels to the intestinal lumen, are less sensitive to colitis than control mice. We found hREG3A to alter the colonic microbiota by decreasing levels of ROS. Fecal microbiota from *REG3A*-TG mice protect non-TG mice from induction of colitis. These findings indicate a role for reduction of oxidative stress in preserving the gut microbiota and its ability to prevent inflammation.

Keywords: Mouse Model; IBD; Bacteria; LPS.

EDITOR'S NOTES

BACKGROUND AND CONTEXT

Paneth's cells release a wide variety of C-type lectins and antimicrobial peptides into the intestinal lumen, but we do not know how they contribute to gut microbiota preservation and inflammation prevention.

NEW FINDINGS

The researchers show that the lectin REG3A reduces oxidative stress for the gut epithelium and the commensal bacteria that form the gut microbiota and thus attenuates inflammation in mice with colitis.

LIMITATIONS

This study did not determine which sites of REG3A are involved in free-radical scavenging.

IMPACT

The enteric delivery of REG3A is a promising therapeutic method for the management of IBD.

An abnormal gut microbiota composition (dysbiosis) and defective antimicrobial mucosal barrier are important pathogenic factors for inflammatory bowel diseases (IBDs).¹ Dysbiosis was reported to occur before clinical symptoms in pediatric Crohn's disease, suggesting that dysbiosis contributed to disease onset in genetically susceptible individuals.² Dysbiosis associated with IBD generally consists of shifts in relative abundance of specific bacterial communities favoring potentially harmful aerobic and facultative anaerobic bacteria to the detriment of beneficial strict anaerobic ones.³ There is accumulating evidence that these shifts result from the oxidative nature of the host inflammatory response.^{4,5} The selection mechanism is that oxidized by-products of the host inflammatory response feed aerobic and facultative anaerobic bacteria, while the strict anaerobic bacteria, which lack reactive oxygen species (ROS) detoxifying enzymes, are killed. Oxidative stress in the gastrointestinal tract (GIT) is thus closely linked to dysbiosis during IBD and non-IBD gut disorders and might be an important therapeutic target.^{6,7}

Another key contributor to dysbiosis and mucosal barrier impairment during IBD is a deficiency in the secretion of antimicrobial proteins (AMPs) such as defensins, cathelicidins, and C-type lectins resulting notably from Paneth cell dysfunction.⁸ This enteric arsenal forms part of innate immunity, contributing to a balanced clearance of pathogens and tolerance of commensal microbes in the gut.^{8,9} In mice, an overexpression, or an oral administration, of an enteric defensin led to significant changes in gut microbiota composition; however, the underlying mechanisms and the health benefits provided by these changes remain to be demonstrated.^{10,11} In fact, AMPs display multiple biological activities, each of which might influence the host-microbiota interplay,¹² but those by which they actually regulate the gut microbiota composition and function are little known. In particular, the way in which the antimicrobial properties of AMPs interact with such a complex ecosystem as the gut microbial communities remains unclear, given that these

antimicrobial properties are counteracted by various mechanisms of bacterial resistance that maintain homeostasis.^{13,14} Moreover, an individual antimicrobial molecule only targets a narrow bacterial spectrum, so that a broad range of them must act simultaneously to ensure selection pressure on the gut microbiota.¹⁵ The structure and function of some antimicrobial molecules are sensitive to environmental factors, such as pH and redox potential,¹⁶⁻¹⁸ entailing that a given set of molecules exerts different selection pressures in homeostatic or inflammatory states.

The human secreted C-type lectin hREG3A (human regenerating family member 3 alpha), or hepatocarcinoma-intestine-pancreas/pancreatitis-associated protein, is a 16-kDa carbohydrate-binding protein exhibiting remarkable anti-inflammatory activities in many eukaryote cell types, where hREG3A promotes tissue regeneration and repair.¹⁹⁻²⁵ It is expressed in Paneth's cells and the neuroendocrine cells of the small intestine physiologically, and in the large intestine in response to infection and inflammation. The mechanisms of reduction of inflammation by hREG3A are not fully understood. hREG3A is a potent ROS scavenger and its tissue-protective and regenerative effects are largely due to this antioxidant property.^{19,20,25} hREG3A and its murine homologue Reg3g also display antibacterial activities against gram-positive bacteria by interacting with peptidoglycan carbohydrate.²⁶ Reg3b, another murine homologue of hREG3A, exerts bactericidal activity against gram-negative bacteria by binding to lipopolysaccharide.²⁷⁻²⁹ Strain differences in susceptibility of gram-positive bacteria to hREG3A have been reported,^{30,31} suggesting that the antibacterial spectrum of the REG3 (regenerating islet-derived protein 3) proteins might be relatively narrow.

In this study, we investigated the effects of an enteric delivery of the human REG3A protein on gut microbiota homeostasis and the response to inflammation in mice. We showed that hREG3A changed the gut microbiota composition (enrichment of Clostridiales, depletion of Bacteroidetes and Proteobacteria), decreased the oxidative stress and inflammatory response of the gut epithelium, and reduced host susceptibility to colitis. hREG3A lowered ROS levels in the gut microbiota of mice with colitis and increased the viability of some gram-positive oxygen-sensitive *Clostridia* in vitro, indicating that the antioxidant activity of hREG3A contributed to shaping the gut microbiota. This study offers

*Authors share co-first authorship.

Abbreviations used in this paper: AMPs, antimicrobial peptides/proteins; DSS, dextran sodium sulfate; ExGF, formerly germ-free; [¹⁸F]FDG, 2-[¹⁸F] fluoro-2-deoxy-D-glucose; H₂-DCFDA, 2',7'-dichlorofluorescein diacetate; hREG3A, human regenerating family member 3 alpha; IBD, inflammatory bowel disease; GIT, gastrointestinal tract; LPS, lipopolysaccharide endotoxin; PCA, principal component analysis; rcREG3A, recombinant human REG3A protein; REG3, regenerating islet-derived protein 3; ROS, reactive oxygen species; rRNA, ribosomal RNA; TG, transgenic; TNBS, 2,4,6-trinitrobenzene sulfonic acid; WT, wild-type.

 Most current article

© 2018 by the AGA Institute. Published by Elsevier Inc. This is an open access article under the CC BY-NC-ND license (<http://creativecommons.org/licenses/by-nc-nd/4.0/>).

0016-5085

<https://doi.org/10.1053/j.gastro.2017.11.003>

a new paradigm for regulation of the host-microbiota interplay based on the ROS scavenging activity of an innate immune molecule.

Materials and Methods

Animal Studies

Animal studies were performed in compliance with the institutional and European Union guidelines for laboratory animal care and approved by the Ethics Committee of CE2A-03-CNRS-Orléans (Accreditation N°01417.01). Homozygous transgenic (TG) C57BL/6 mice expressing *REG3A* in hepatocytes under the control of the mouse albumin gene promoter were derived from a strain previously produced in our laboratory.³² The cohousing experiments were performed with 3-week-old weaned wild-type (WT) mice randomly cohoused with age-matched *REG3A*-TG mice at a 1:1 ratio for 8 weeks. Ten-week-old germ-free mice underwent 2 gastric gavages at 48-hour intervals using inocula consisting of pooled fresh feces from 8 *REG3A*-TG or WT mice.

Dextran Sodium Sulfate Colitis

Colitis was induced in mice with a 3% 40 kDa dextran sodium sulfate (DSS) solution (TdB Consultancy AB, Uppsala, Sweden), which was added to their drinking water for 5 days followed by ad libitum access to tap water for 7 days.

2,4,6-Trinitrobenzene Sulfonic Acid Colitis

Overnight-fasted mice were anesthetized for 90 minutes and received intrarectally 150 mg/kg of 2,4,6-trinitrobenzene sulfonic acid (TNBS; Sigma-Aldrich, St Louis, MO) together with ethanol. WT mice received an intrarectal injection of 100 μ g of a recombinant hREG3A protein on the day before and on the day of TNBS administration.

16S Ribosomal RNA Analysis

DNA pyrosequencing of the V3-V4 hypervariable region of 16S ribosomal RNA (rRNA) gene was performed using the Illumina MiSeq instrument (San Diego, CA). The sequences thus generated were pre-processed using the mothur pipeline and then clustered into operational taxonomic units based on 97% of similarity. RDP release 11 was used as reference database. Principal component analysis (PCA) was performed based on bacterial family and genera compositions using the R packages ade4 and FactoMiner.

Bacterial Strains, Culture Conditions, and ROS Quantification

The bacterial strains used were *Enterococcus faecalis* (ATCC-19433), *Faecalibacterium prausnitzii* A2-165 (DSM17677), and *Roseburia intestinalis* L1-82 (DSM14610T). Oxidative stress was induced by addition of 200 mM paraquat (1,1'-dimethyl-4,4'-bipyridinium dichloride; Sigma-Aldrich), which is commonly used experimentally to generate superoxide radical, hydrogen peroxide, and hydroxyl radical in cells.³³ Intracellular ROS levels and cell viability were determined by flow cytometry with 2',7'-dichlorofluorescein diacetate (H₂-DCFDA) and propidium iodide in bacteria cultures. Bacterial growth was assessed by colony-forming unit counting on

agar plates. Bacterial ROS levels in fresh fecal microbiota were measured by flow cytometry with H₂-DCFDA.

Other Methods

For histology, immunohistochemistry, recombinant protein production, enzyme-linked immunosorbent assays, immunoblotting, dot-blot, fluorescence in situ hybridization, transcriptomics, and 2-[¹⁸F]fluoro-2-deoxy-D-glucose ([¹⁸F]FDG) positron emission tomography scan, please see details in the [Supplementary Materials and Methods](#).

Statistics

Results are presented as means \pm SEM or box plots. Differences between sample groups were tested using nonparametric Wilcoxon rank sum (2-sided) for all the experiments reported, except for the following: 2-way analysis of variance tests were used for the in vivo quantifications of [¹⁸F]FDG and H₂-DCFDA over time; the robustness of PCA clustering was assessed with a Monte-Carlo rank test; and the Kaplan-Meier survival analysis with a log-rank test was applied to compare the time course of survival between the groups. *P* values less than 0.05 were deemed statistically significant.

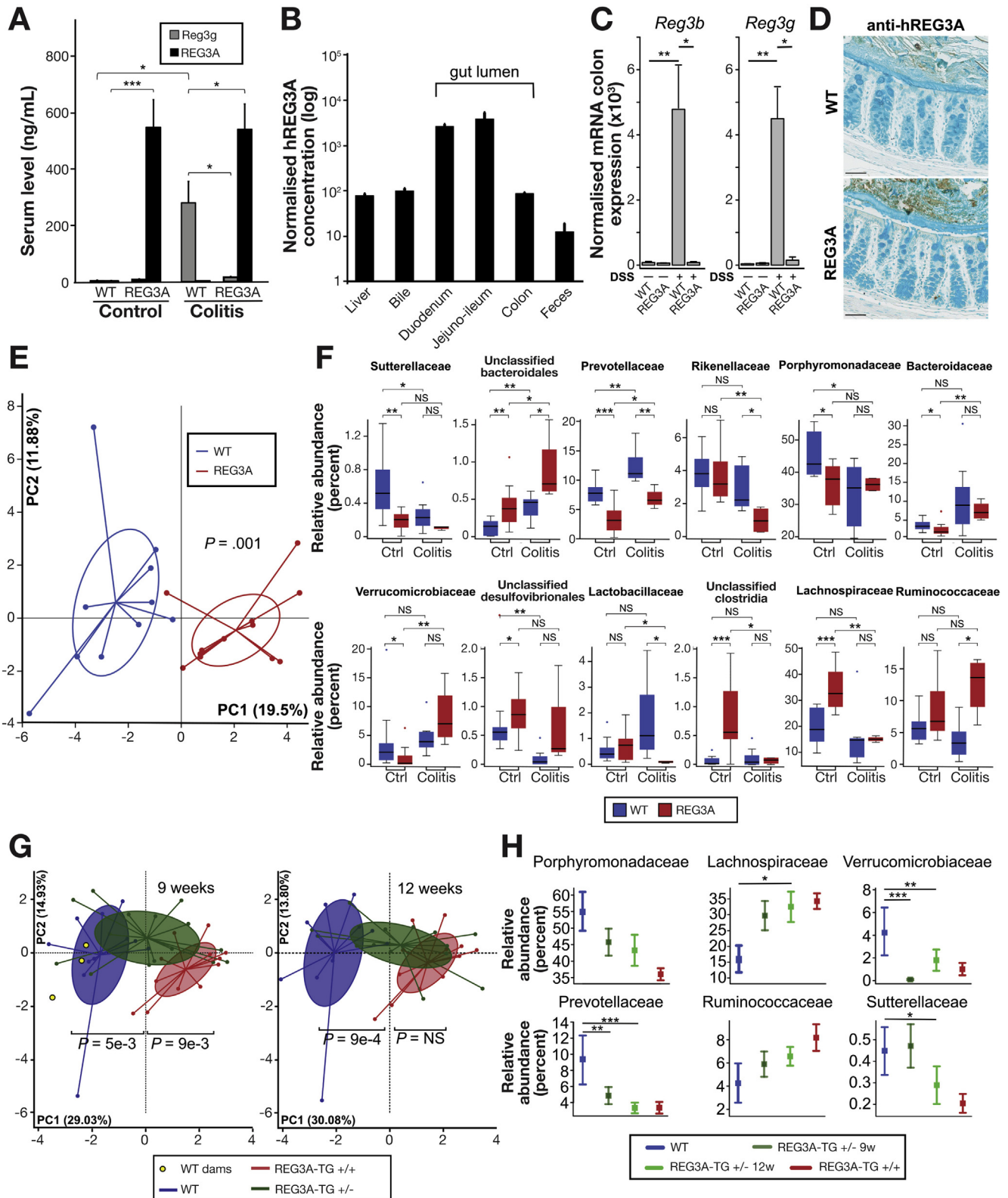
Results

Human REG3A Delivered into the Gut Lumen Shifts the Gut Microbiota Composition in Hepatocyte-targeted REG3A Transgenic Mice

We studied the effects of human REG3A on gut microbiota composition and gut barrier integrity in mice TG for *REG3A* under homeostatic and inflammatory conditions. Inflammation was induced by oral absorption of DSS. To prevent degradation of the hREG3A protein by acid and luminal proteases in the upper GIT, we used previously generated homozygous TG C57BL/6 mice expressing *REG3A* in hepatocytes under the control of the mouse albumin gene promoter³² and showed that, in these mice, hREG3A flowed into bile ducts and the GIT lumen ([Figure 1A, B, and D](#)). Transgenic hepatocytes secreted hREG3A into blood vessels through the basolateral membranes, and into bile canaliculi through the apical membranes. The expression levels of endogenous Reg3b and Reg3g in the blood and colon tissues were negligible in the basal state of WT mice and high after DSS administration ([Figure 1A and C](#)). In *REG3A*-TG mice, a similar high serum level of hREG3A was found in the basal and inflammatory states ([Figure 1A](#)). This level was similar to that of the endogenous Reg3 in WT mice with colitis. The colon expression levels of the endogenous Reg3 mRNAs were negligible in both the basal and inflammatory states of *REG3A*-TG mice ([Figure 1C](#)). In other words, *REG3A*-TG mice did not display any up-regulation of Reg3b or Reg3g during colitis (perhaps because they were retro-controlled by the overexpressed *REG3A*), implying that Reg3b and Reg3g played a negligible part in *REG3A*-TG mice. We analyzed the fecal microbiota composition in healthy and DSS-given *REG3A*-TG mice using MiSeq 16S rDNA gene sequencing. Control WT and *REG3A*-TG mice were bred and processed under the same conditions. PCA revealed 2 clearly separate clusters for *REG3A*-TG and WT mice at the family level both

before ($P = .001$) and after ($P = .039$) exposure to DSS (Figure 1E and Supplementary Figure 1A). Twelve bacterial families displayed significant differences in their relative abundance between REG3A-TG and WT mice in either the

basal or inflammatory state, or both (Figure 1F). Sutterellaceae (phylum Proteobacteria), Prevotellaceae, Porphyromonadaceae, and Bacteroidaceae (phylum Bacteroidetes) were underrepresented, whereas Lachnospiraceae and



unclassified *Clostridia* (phylum Firmicutes) were over-represented in the basal state of *REG3A*-TG mice compared with that of WT mice (Figure 1F). The same shifts in microbial composition were found at the genus level (Supplementary Figure 1B). In the inflammatory, compared with basal, state, WT mice displayed an enrichment of Prevotellaceae and unclassified Bacteroidales, and a depletion of Porphyromonadaceae, Sutterellaceae, and unclassified Desulfovibrionales, whereas *REG3A*-TG mice displayed an increase in Prevotellaceae, unclassified Bacteroidales, Bacteroidaceae, and Verrucomicrobiaceae and a decrease in Lactobacillaceae, unclassified *Clostridia* and Lachnospiraceae. DSS-given *REG3A*-TG mice exhibited a lower level of Prevotellaceae and a much higher level of Ruminococcaceae (order Clostridiales) (Figure 1F and Supplementary Figure 1C) than DSS-given WT mice. We then investigated whether the gut microbiota composition of homozygous TG (*REG3A*-TG+/+) mice at baseline was due to the *REG3A* transgene or an extra-genetic effect.³⁴ We studied the time evolution of the microbiota in mice that expressed only 1 copy of human *REG3A* transgene (*REG3A*-TG+/-), were born to WT mothers and initially had the maternal microbiota. The fecal microbiomes of 15 *REG3A*-TG+/- pups from 3 different litters and cages were sequenced at the ages of 9 and 12 weeks and compared with those of their WT dams (n = 3) and unrelated WT mice of similar ages (n = 11). The fecal microbiomes of 12 *REG3A*-TG+/+ mice were analyzed for comparison. PCA plots at the family level showed that the microbiota from *REG3A*-TG+/- mice were grouped in-between those from (maternal and unrelated) WT and *REG3A*-TG+/+ mice at 9 weeks ($P < .01$ for *REG3A*-TG+/- vs WT and *REG3A*-TG+/- vs *REG3A*-TG+/+) and moved close to those from *REG3A*-TG+/+ mice during the next 3 weeks ($P < .001$ for *REG3A*-TG+/- vs WT; $P > .05$ for *REG3A*-TG+/- vs *REG3A*-TG+/+) (Figure 1G). The microbiota composition shift of the *REG3A*-TG+/- mice compared with the microbiota of WT mice mostly consisted of a decrease in Prevotellaceae, Sutterellaceae, and Verrucomicrobiaceae, and an increase in Lachnospiraceae and Ruminococcaceae, to reach levels comparable to those of *REG3A*-TG+/+ mice after 12 weeks (Figure 1H). Thus, the WT microbiota of the *REG3A* heterozygous newborns evolved toward a TG-positive microbiota in a few months, which means that the *REG3A* transgene effect superseded the maternal legacy.

hREG3A Increases the Viability of Some Highly Oxygen-Sensitive *Clostridia*

The shift in microbiota composition in *REG3A*-TG mice compared with WT mice corresponded to a large increase in the ratio between gram-positive and gram-negative bacteria (Figure 2A), difficult to reconcile with the reported selective anti-gram-positive bactericidal activity of *hREG3A*.²⁶ We conjectured that the antioxidant activity of *hREG3A* was a key factor in shifting the intestinal microbial ecology in *REG3A*-TG mice. The mechanism at play would be a selection pressure exerted by *hREG3A* in favor of strict anaerobic gram-positive bacteria, as are some *Clostridia*. To substantiate this view, we measured ROS levels in fresh fecal microbiota of WT and *REG3A*-TG mice using H₂-DCFDA and flow cytometry over the 5-day period of DSS administration, during which the gut barrier was not yet damaged nor colitis established. The ROS levels at day 1 of DSS administration were similar to the baseline level and then increased over time in both mouse lines. However, the rate of increase was significantly lower for the microbiota of *REG3A*-TG mice ($P = .02$ over the day 1–5 period), evidencing a ROS scavenging activity of the *REG3A* transgene in a microbiota subjected to an oxidative stress (Figure 2B). We also tested the antioxidant efficiency of a full-length recombinant human *REG3A* protein (rc*REG3A*) in prokaryote cells in vitro. The recombinant protein we used is chemically and biologically active in terms of anti-inflammatory properties in eukaryotic cells and carbohydrate-binding selectivity^{10,20,25} (Supplementary Figure 2). We cultured gram-positive *Enterococcus faecalis* stressed with a ROS generator (paraquat) during the exponential phase of growth. Exposure to 200 mM paraquat had a strong bactericidal effect on *E faecalis*. The addition of 10 μM rc*REG3A* restored the exponential growth of *E faecalis*, suggesting that the ROS generated by paraquat were effectively reduced by rc*REG3A* (Figure 2C). This was demonstrated by flow cytometry using the ROS-specific fluorescent probe H₂-DCFDA and propidium iodide DNA staining (Figure 2D and E and Supplementary Figure 3). We found some bacterial aggregation, but no bactericidal effect of rc*REG3A* on *E faecalis* (Figure 2C), at variance with previous reports.²⁶ This discrepancy may rely on many factors pertaining to the protein²⁶ or the bacterial strain,^{30,31} but note that an absence of bactericidal activity of *hREG3A* would be consistent with the enrichment of gram-positive bacteria we

Figure 1. *hREG3A* shapes gut microbiota in *REG3A*-TG mice. (A) Serum concentrations of human *REG3A* and murine *Reg3g* in WT and *REG3A*-TG mice (*REG3A*) before (Control) and after (Colitis) administration of DSS (n = 6). (B) Digestive tract concentrations of *hREG3A* (n = 3). (C) Colonic *Reg3b* and *Reg3g* mRNA expression level (n = 5). (D) Alcian blue and anti-*hREG3A* stainings of colon tissue sections. Scale bar, 100 μm. (E) PCA of bacterial profiles at the family level in the fecal microbiota of *REG3A*-TG (n = 12) and WT (n = 10) mice in the basal state. Each dot represents 1 mouse. $P = .001$ (Monte-Carlo rank test). (F) Relative abundances of bacterial families in the basal state (Ctrl) of the same mouse cohorts as in (E) and on day 12 after onset of exposure to DSS (Colitis) in *REG3A*-TG (n = 5) and WT (n = 7) mice. (G) PCA of bacterial profiles at the family level in heterozygous (*REG3A*-TG+/-; n = 15), homozygous (*REG3A*-TG+/+; n = 12), and unrelated WT (n = 11) mice of similar ages (Monte-Carlo rank test). Each dot represents 1 mouse. Yellow dots: WT dams of the *REG3A*-TG+/- mice (n = 3). (H) Relative abundances of bacterial families in *REG3A*-TG+/- mice aged 9 and 12 weeks compared with WT (n = 14) and to *REG3A*-TG+/+ mice. The data are averages ± SEM. Except for (E) and (G), the 2-sided Wilcoxon rank sum test was performed for analysis. * $P < .05$, ** $P < .01$, *** $P < .001$.

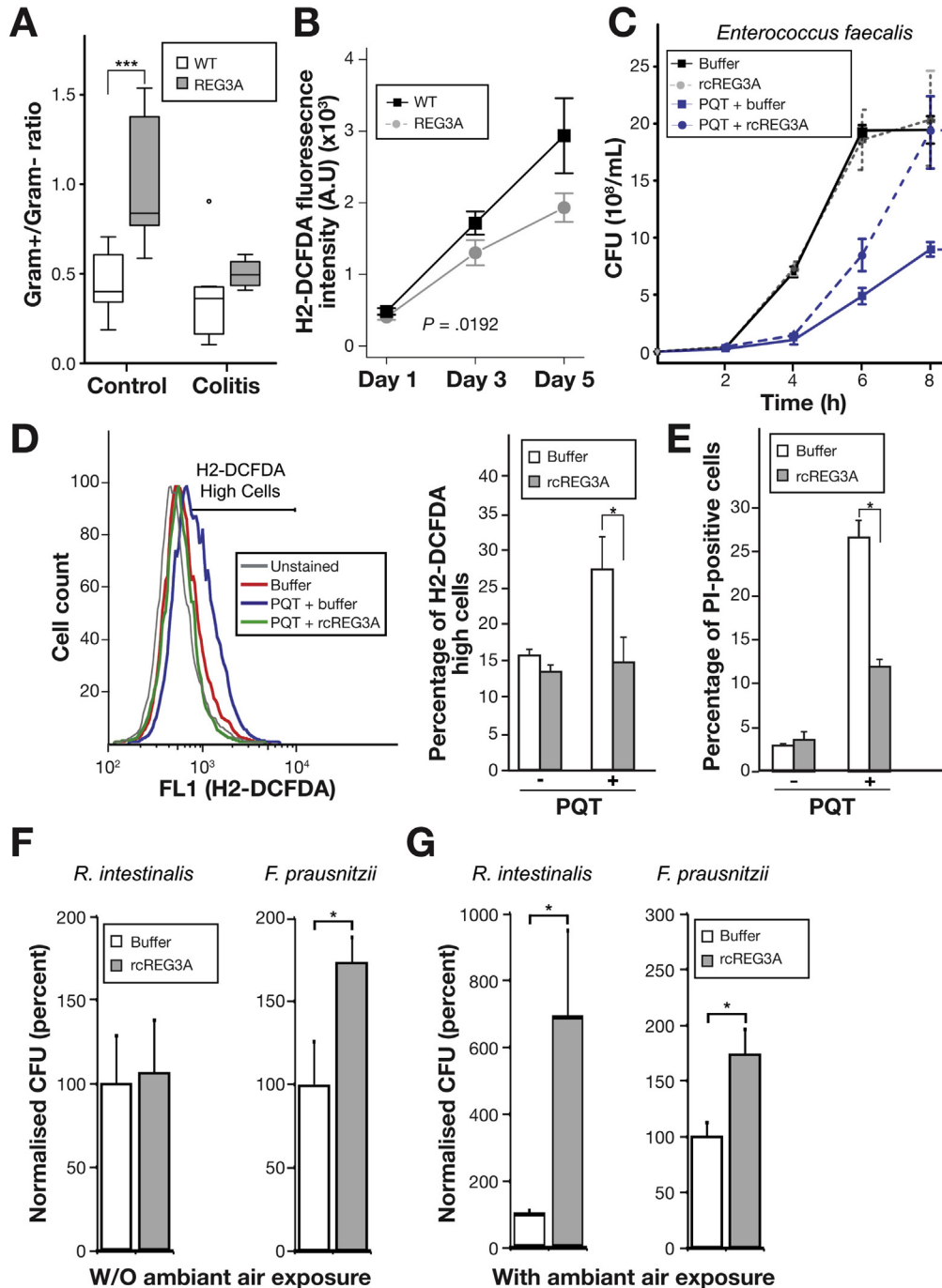


Figure 2. hREG3A rescues bacteria from oxidative stress. (A) Ratio of gram-positive to gram-negative bacteria in the fecal microbiota of REG3A-TG (REG3A) and WT mice in the basal state (control) and on day 12 of induced colitis. Same cohorts as in Figure 1E and F. (B) Bacterial ROS levels in the fecal microbiota of REG3A and WT mice ($n = 6$ per group) measured by flow cytometry and H₂-DCFDA during the period of DSS administration. $P = .019$ (2-way analysis of variance). (C) Growth of gram-positive *Enterococcus faecalis* under oxidative stress. CFU, colony-forming units; PQT, paraquat. Assays were done in quadruplicate in 3 independent experiments. (D) Cellular ROS levels in *E. faecalis* cultures measured by flow cytometry with H₂-DCFDA. Left: Representative flow cytometry curves. H₂-DCFDA high cells: the 15% most strongly fluorescent cells in the PQT + buffer condition. Right: Percentage of bacteria in the high-intensity range in 3 independent experiments. (E) Cell viability by flow cytometry with propidium iodide (PI). Normalized CFU numbers of gram-positive *Roseburia intestinalis* and *Faecalibacterium prausnitzii* in strictly anaerobic cultures (F) and after exposure to ambient air (G). The numbers of CFUs were normalized to the average CFU number measured in control cultures (buffer). Assays were done in quadruplicate in 2 independent experiments. The data are averages \pm SEM. The 2-sided Wilcoxon rank sum test was performed for analysis except for (B). * $P < .05$, *** $P < .001$.

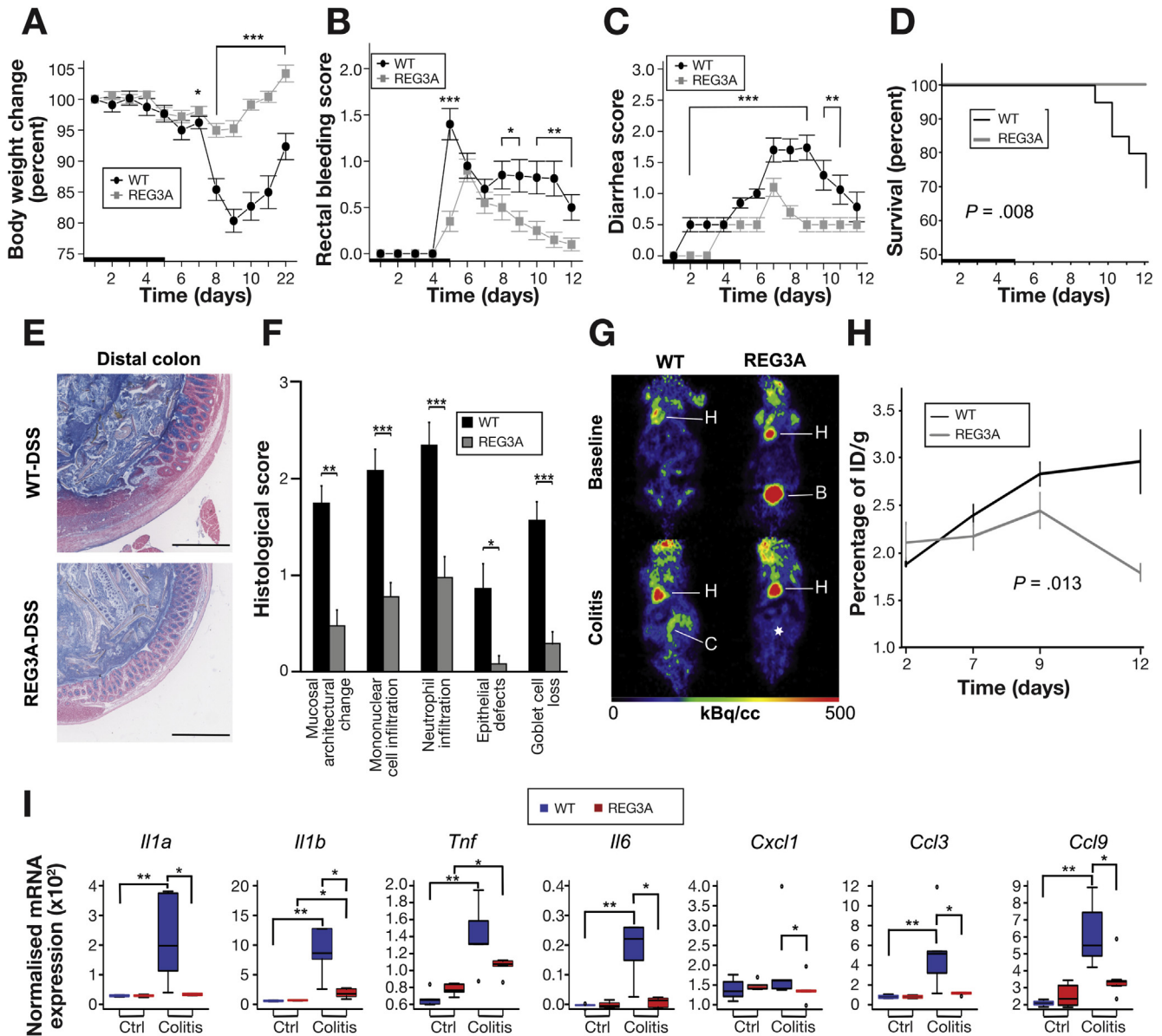


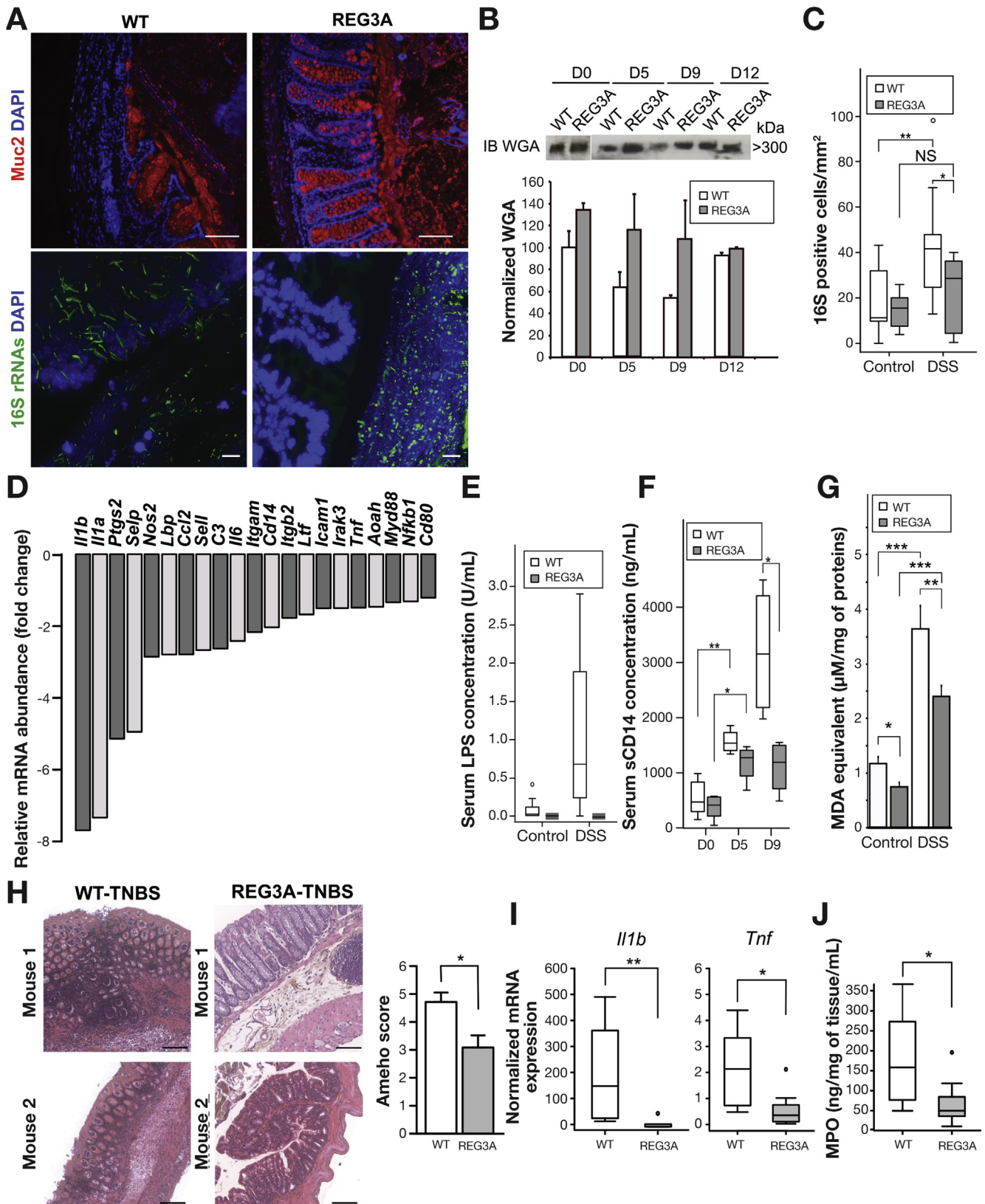
Figure 3. *REG3A*-TG mice have a lower susceptibility to DSS-induced colitis than WT mice. (A–D) Time evolution of DSS-induced colitis in *REG3A*-TG (*REG3A*) and WT mice (n = 20 for each group; 2 independent experiments). Heavy line: 5-day period of DSS administration. (A) Body weight change. (B) Rectal bleeding score. (C) Diarrhea score. (D) Kaplan-Meier survival plot. (E) Representative day-12 colon images stained with hematoxylin-eosin and Alcian blue. Scale bar, 50 μ m. (F) Histological assessment of gut epithelium (n = 14 for each group). (G) Representative whole-body [¹⁸F]FDG positron emission tomography images. The images are frontal slices of 3-dimensional volumes passing through heart, B, bladder; C, colon; H, heart. *Absence of colon uptake. (H) Quantification of [¹⁸F]FDG over time (n = 3). $P = .013$ (2-way analysis of variance). (I) mRNA expression level of the indicated inflammatory markers in colonic epithelial cells of WT and *REG3A*-TG mice (n = 5). The data are means \pm SEM. The 2-sided Wilcoxon rank sum test was performed for analysis except for (H). * $P < .05$, ** $P < .01$, *** $P < .001$.

observed in the gut microbiota of *REG3A*-TG mice compared with that of WT mice. We cultured of 2 well-documented extremely oxygen-sensitive gram-positive bacteria species, *Roseburia intestinalis* (Lachnospiraceae, Clostridium Cluster XIVa) and *Faecalibacterium prausnitzii* (Ruminococcaceae, Clostridium Cluster IV), which are major butyrate producers dramatically reduced during IBD.^{35–38} *R. intestinalis* is known to survive for less than 2 minutes when exposed to air on the surface of agar plates.³⁹ *F. prausnitzii* is more sensitive to air exposure than *R. intestinalis* and grows

slowly even under anaerobic conditions.⁴⁰ We performed anaerobic cultures of *R. intestinalis* and *F. prausnitzii* followed, or not, by a 5-minute exposure to ambient air. We found that rcREG3A had a significant growth-promoting effect on *F. prausnitzii* under strict anaerobic conditions and a survival effect on both bacteria after exposure to oxygen (Figure 2F and G). The centrifugation of *F. prausnitzii* anaerobic cultures incubated with rcREG3A for 24 hours, followed by anti-hREG3A immunoblotting, showed that a 15-kDa rcREG3A co-sedimented with bacterial aggregates

(Supplementary Figure 4A). Slide-mounted imaging showed that *F. prausnitzii* incubated with rcREG3A survived, whereas control cultures were completely lysed, after 2

hours of exposure to ambient air (Supplementary Figure 4B). These findings establish that rcREG3A exerts a potent antioxidant activity on prokaryotic cells and is



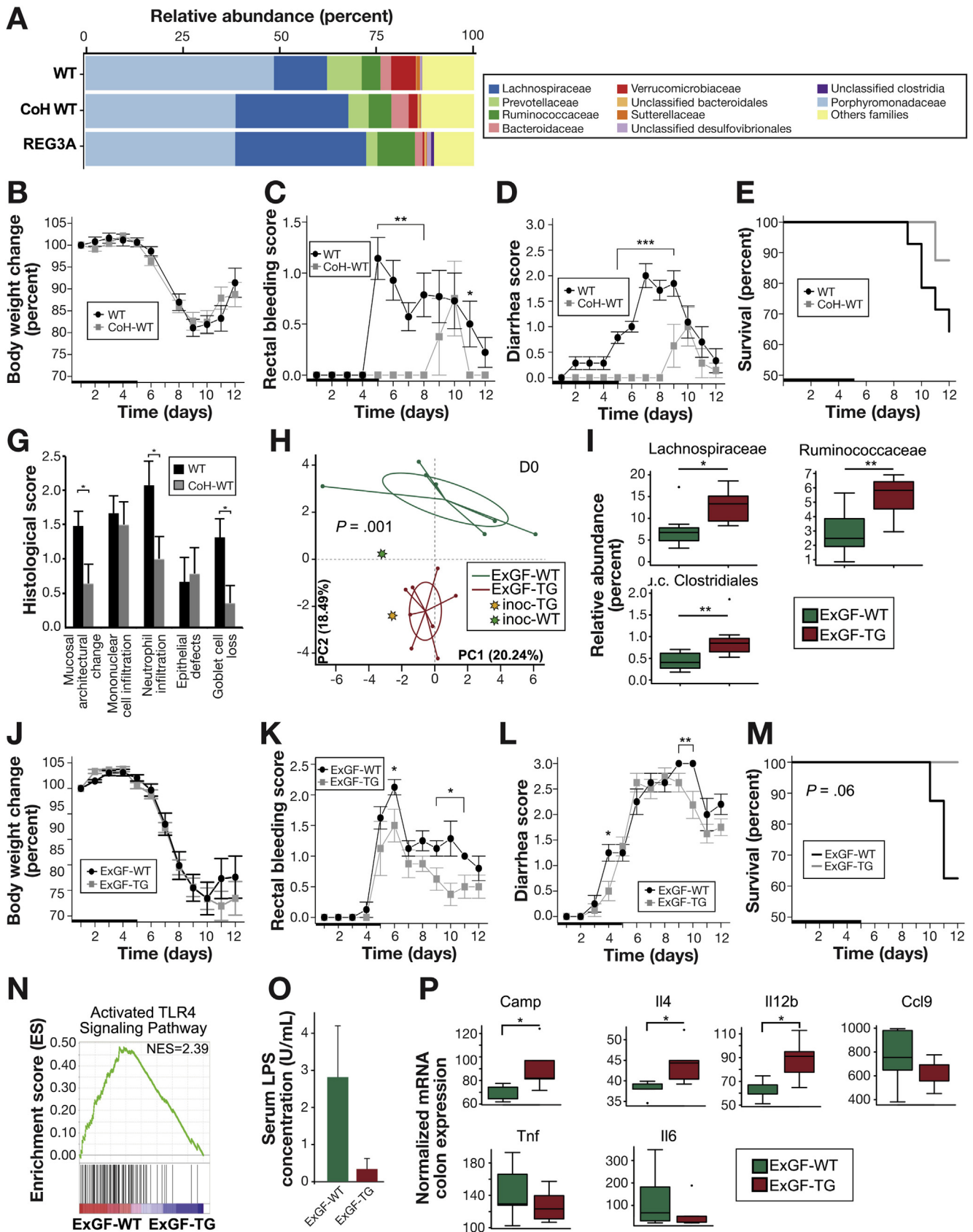
capable of increasing the viability and growth of some extremely oxygen-sensitive commensal Clostridia.

REG3A-TG Mice Are Less Susceptible to DSS- and TNBS-induced Colitis Than WT Mice

The dysbiotic microbiota of patients with IBD is mostly characterized by an increase in Sutterellaceae, Prevotellaceae, and Enterobacteriaceae (phylum Proteobacteria), and a decrease in Ruminococcaceae and Lachnospiraceae (which include the principal butyrate-producing symbionts).^{3,35–38} Similar shifts in the composition of the gut microbiota also are associated with colitis in genetically susceptible mouse models.^{41,42} The fact that more or less reverse shifts occur in the gut microbiota of healthy REG3A-TG mice compared with WT mice suggests that a microbiota shaped by hREG3A might have a beneficial impact on health. We therefore studied the response to induced colitis in REG3A-TG mice, and also performed feces transfer experiments. REG3A-TG mice received oral administrations of 3% DSS for 5 days followed by normal water for 7 days. Control groups of WT mice were bred and processed under the same conditions. Body weight changes, stool consistency, and bleeding scores and survival rate were monitored over time. Histopathological features were scored on day 12. Strikingly, DSS-given REG3A-TG mice displayed only a very few signs of colitis. They had reduced weight loss, diarrhea, and rectal bleeding compared with WT mice and had a 100% survival rate on day 12 compared with 70% in WT mice (Figure 3A–D). Their colons displayed fewer barrier defects and less Goblet cell loss and inflammatory cell infiltration than those of WT mice (Figure 3E and F and Supplementary Figure 5). Twelve-week-old REG3A-TG+/- mice born to WT mothers were also exposed to DSS. They exhibited a relatively benign colitis (Supplementary Figure 6A–D), consistent with the fact that their gut microbiota was similar in composition (Figure 1G), and thus functionality, to those of REG3A homozygous TG mice. We ensured that the hREG3A lectin did not interact with dextran in vitro (Supplementary Figure 2),⁴³ and that, therefore, the observed phenotype could not be attributed to a direct blocking of DSS toxicity by hREG3A. Positron emission tomography imaging with [¹⁸F]FDG, a tracer for abnormally high glucose metabolism in inflammatory areas, was used to quantify intestinal inflammation. Colonic [¹⁸F]FDG uptake increased over time in WT mice with colitis, whereas it remained weak (ie, comparable to that

seen in healthy) in REG3A-TG mice ($P = .013$ over the day 7–12 period) (Figure 3G and H). The severity of colitis also was assessed by measuring the colonic expression levels of inflammatory markers (*Il1a*, *Il1b*, *Tnf*, *Il6*, *Cxcl1*, *Ccl3*, *Ccl9*). Most of them showed a significant increase on DSS administration in WT mice, and not in REG3A-TG mice (Figure 3I). We studied the integrity of the gut mucosal barrier in healthy and DSS-given REG3A-TG mice using immunostaining for Muc2 mucin and 16S rRNA fluorescence in situ hybridization, transcriptome profiling, and gene set enrichment analysis with the KEGG and Reactome databases. In the basal state, mucosal barriers of REG3A-TG and WT mice were microscopically similar. However, several pathways related to the intestinal barrier, including modulators of cell-matrix interactions and mucin *O*-glycosylation, were up-regulated in REG3A-TG mice (Supplementary Figure 7A). During intestinal inflammation, the colon mucosal barrier remained intact over considerable areas in REG3A-TG mice, whereas it was largely disrupted in WT mice, leading to bacterial colonization across the epithelium (Figure 4A). The functional robustness of the mucosal barrier in REG3A-TG, compared with WT, mice was further highlighted as follows. An up-regulation of some tight-junction genes involved in the regulation of cell-cell interactions was observed (Supplementary Figure 7B). An increase in *O*-glycosylation of epithelial mucins was revealed by wheat germ agglutinin immunoblotting (Figure 4B). The level of bacterial translocation in mesenteric lymph nodes remained low, as shown by 16S rRNA fluorescence in situ hybridization analysis (Figure 4C). A number of genes related to the lipopolysaccharide endotoxin (LPS)-induced activation pathway were down-regulated in colon epithelial cells (Figure 4D). Unsupervised transcriptome analysis revealed a clustering of DSS-given REG3A-TG mice with healthy mice separately from DSS-given WT mice (Supplementary Figure 8). Consistent with this, the increase in inflammation-associated serum markers (LPS, soluble CD14) remained very small in these mice during intestinal inflammation (Figure 4E and F). Finally, the concentration of malondialdehyde, a biomarker of oxidative stress, in the colon tissue was substantially reduced in REG3A-TG, compared with WT, mice with colitis (Figure 4G). We then studied the susceptibility of REG3A-TG mice to an alternative type of colitis using a single intrarectal administration of trinitrobenzenesulfonic acid (TNBS) together with ethanol. In contrast with oral administration of DSS, which destroys colon epithelial cells, alters barrier function, and subsequently

Figure 4. Gut barrier integrity and weak inflammation in REG3A-TG mice exposed to DSS or TNBS. (A–G) Mice exposed to DSS. (A) Anti-MUC2 mucin immunofluorescence, bacterial 16S rRNA fluorescence in situ hybridization and 4',6-diamidino-2-phenylindole (DAPI) images of colon tissues from WT and REG3A-TG mice on day 12 of DSS-induced colitis. Scale bars, 20 μ m. (B) Representative anti-wheat germ agglutinin immunoblots (IB WGA) at the indicated time points of DSS-induced colitis. Bar chart: densitometric analysis ($n = 5$ for each group; 2 independent experiments). (C) Bacterial translocation in mesenteric lymph nodes before ($n = 4$) and during colitis ($n = 5$). (D) Changes in expression level of the genes related to the LPS-induced activation pathway that were the most down-regulated in REG3A-TG mice. (E) Serum levels of LPS ($n = 8$). (F) Serum levels of soluble CD14 ($n = 8$). (G) Concentration of malondialdehyde (MDA) in gut epithelium extracts ($n = 9$ –14). (H–J) Mice exposed to TNBS. REG3A-TG and WT mice were administered TNBS together with ethanol intrarectally ($n = 15$ per group). (H) Ameho quantitative histological score and 2 representative histological examinations for each group 2 days after TNBS administration. Scale bar, 100 μ m. (I) mRNA expression level of the *Il1b* and *Tnf* inflammatory cytokines. (J) Myeloperoxidase (MPO) concentration in colon tissue extracts. The data are represented either as box plots or means \pm SEM. The 2-sided Wilcoxon rank sum test was performed for analysis. * $P < .05$, ** $P < .01$, *** $P < .001$.



causes inflammation, TNBS rapidly triggers a severe colonic inflammation through a T-cell immune response against haptenized proteins and luminal antigens.⁴⁴ We found that, 2 days after TNBS administration, *REG3A*-TG mice developed only mild colonic inflammation and mucosal damage (Figure 4H) associated with decreased levels of inflammatory cytokines (*Il1b*, *Tnf*) and myeloperoxidase (Figure 4I and J).

The Anti-inflammatory Properties of Gut Microbiota Shaped by hREG3A Promote Survival to DSS-induced Colitis in Colonized WT Mice

To assess the protective action of hREG3A-shaped microbiota against colitis, we transferred fecal microbiota from *REG3A*-TG mice to WT mice by means of cohousing. Three-week-old weaned WT mice were cohoused with age-matched *REG3A*-TG mice for 8 weeks and then exposed to DSS. Control groups consisted of WT mice housed alone. At the end of the cohousing period, cohoused-WT mice displayed a significant shift in gut microbiota composition toward an *REG3A*-TG profile at the bacteria family level (Figure 5A) and a clear alleviation of DSS-induced colitis compared with single-housed WT mice (Figure 5B–G). Next, we colonized germ-free C57BL/6 mice with a fecal microbiota from *REG3A*-TG or WT mice for 3 weeks. Formerly (Ex) germ-free (GF), but now colonized, mice will be designated as ExGF-TG or ExGF-WT according to the origin of the colonizing microbiota. The fecal microbiota was then analyzed by sequencing (day 0) and colonized mice were exposed to DSS. The microbiota of ExGF-TG and ExGF-WT mice at day 0 had somewhat drifted from their respective inocula (Figure 5H). Nevertheless, the microbiota of ExGF-TG mice still harbored the same predominant bacterial communities as the inoculum, albeit with different relative abundance values, and remained far from that of ExGF-WT mice (Figure 5H and I and Supplementary Figure 9A–E). On DSS administration, ExGF-TG mice exhibited a complete colitis survival despite transient signs of colitis, whereas 37% of the ExGF-WT mice died (Figure 5J–M and Supplementary Figure 10). This was associated with a reduced inflammatory response in terms of TLR4 signaling activation, colonic inflammatory markers, and LPS-induced endotoxemia (Figure 5N–P). These results demonstrate a transmissible pro-survival action of the microbiota shaped by hREG3A probably due to a reduced inflammatory

response in the gut epithelium and less systemic dissemination of gram-negative LPS. This is consistent with the depletion of potentially aggressive gram-negative bacteria we observed in the gut microbiota shaped by hREG3A (Figure 2A).

Rectal Use of a Recombinant REG3A Protein Diminishes Colonic Inflammation in Mice With TNBS-induced Colitis

The fact that signs of colitis were partly reduced in cohoused-WT and ExGF-TG mice while they were fully suppressed in *REG3A*-TG mice suggests that, in the latter, a direct interaction between overexpressed hREG3A and the host contributed to the maintenance of gut barrier homeostasis, in addition to the anti-inflammatory effects of the gut microbiota shaped by hREG3A. To substantiate this view, we evaluated the effects of intrarectal administrations of rcREG3A in WT mice with colitis. An amount of 100 μ g of rcREG3A (or an equivalent volume of buffer) was delivered on the day before and on the day of TNBS administration. The body weight loss was the same in the 2 groups of mice (Figure 6A). Histological stainings revealed that mice given intrarectal rcREG3A showed milder colonic barrier defects and inflammation than mice not given intrarectal rcREG3A (Figure 6B and Supplementary Figure 11). A significant decrease of the inflammatory markers *Il1b*, *Tnf*, and myeloperoxidase was observed in the colon tissues of mice given intrarectal rcREG3A (Figure 6C). These positive effects of a local administration of a recombinant REG3A protein make it very likely that the lower susceptibility to colitis observed in *REG3A*-TG mice was mostly due to the hepatic transgene REG3A traveling to the gut lumen, and not to a liver-dependent effect. They indicate that an exogenous hREG3A can contribute to the preservation of gut barrier integrity during colitis and underlines the potential human-health relevance of this molecule.

Discussion

Enteric innate immune molecules play an important role in gut barrier function and gut microbiota homeostasis through their pleiotropic activities. A reduced production of AMPs resulting from a deregulation of the function of Paneth's cell may lead to dysbiosis and ultimately IBD.³

Figure 5. Alleviated colitis severity in conventional and germ-free mice colonized with a hREG3A-shaped microbiota. (A) Relative abundances of bacterial families in the fecal microbiota of WT mice cohoused with *REG3A*-TG mice for 8 weeks (cohoused-WT; n = 8) compared with single-housed WT (n = 10) and *REG3A*-TG (n = 7) mice. (B–E) Time evolution of DSS-induced colitis in cohoused-WT and single-housed WT mice. Heavy line: 5-day period of DSS administration. (B) Body weight change. (C) Rectal bleeding score. (D) Diarrhea score. (E) Kaplan-Meier survival plot (P = nonsignificant). (G) Histological assessment of gut epithelium (n = 5). (H) PCA at the family level of germ-free mice colonized with microbiota from WT (ExGF-WT; n = 8) and *REG3A*-TG (ExGF-TG; n = 8) mice 3 weeks after mice were fed feces (day 0). inoc, inoculum used for oral gavage. P = .001 (Monte-Carlo rank test). (I) Relative abundances of the main bacterial families that are overrepresented in conventional *REG3A*-TG mice at day 0. (J–M) Time evolution of DSS-induced colitis in ExGF-WT and ExGF-TG mice. Heavy line: 5-day period of DSS administration. (J) Body weight change. (K) Rectal bleeding score. (L) Diarrhea score. (M) Kaplan-Meier survival plot. (N) Gene enrichment of TLR4 pathway on day 12 of colitis. NES, normalized enrichment score. (O) Serum LPS levels. (P) mRNA expression level of the indicated pro- and anti-inflammatory markers in colonic epithelial cells of ExGF-WT and ExGF-TG mice (n = 5). The data are averages \pm SEM. Except in (H), the 2-sided Wilcoxon rank sum test was performed for analysis. *P < .05, **P < .01, ***P < .001.

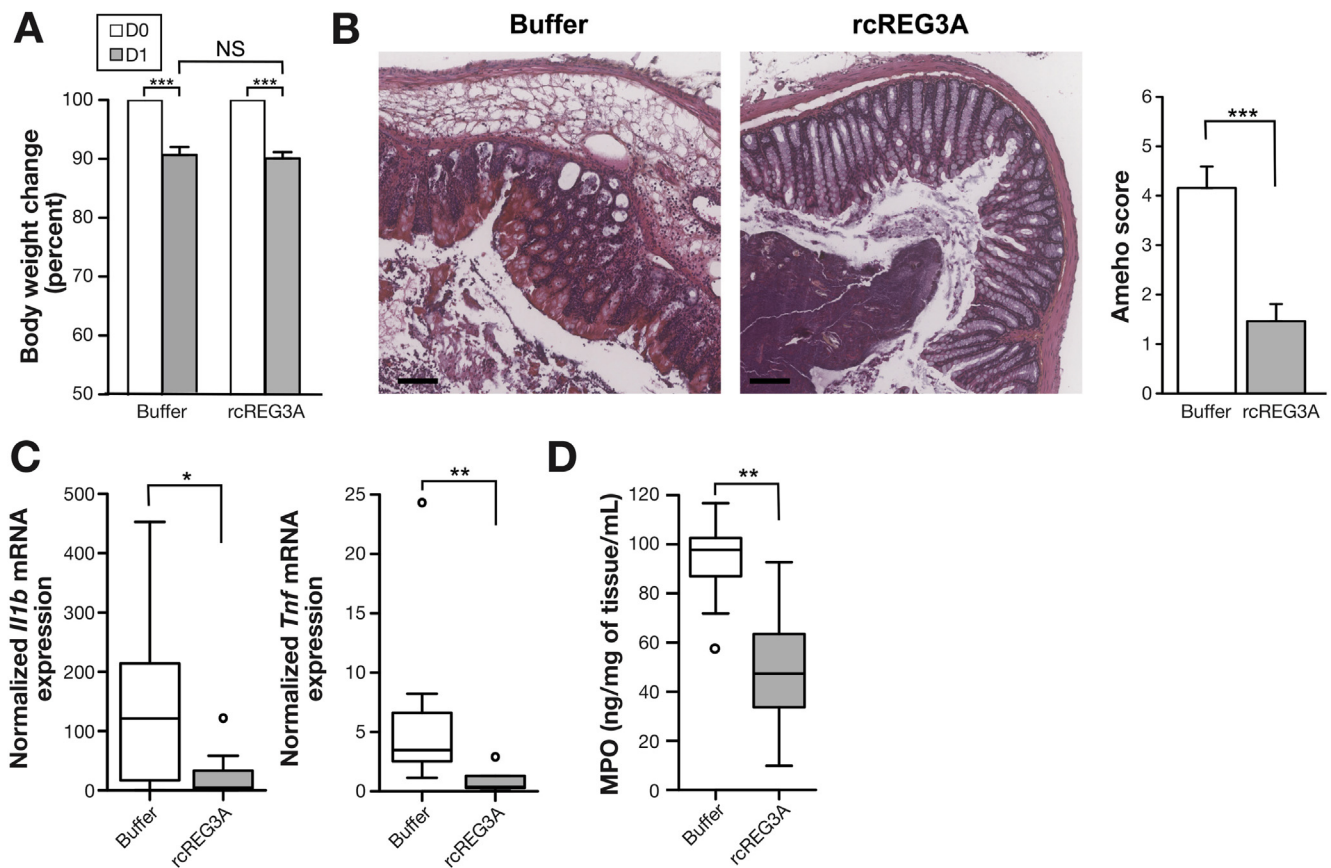


Figure 6. Intrarectal administration of hREG3A decreased colon damage and inflammation in WT mice with colitis. A total of 100 μ g of a recombinant REG3A protein (rcREG3A; n = 14) or an equivalent volume of buffer (n = 15) was administered intrarectally in WT mice with colitis on the day before (D0) and on the day (D1) of TNBS administration. (A) Body weight change. (B) Ameho quantitative histological score and representative colon images stained with hematoxylin and eosin. Scale bar, 100 μ m. (C) Colonic mRNA expression level of *Il1b* and *Tnf*. (D) Myeloperoxidase (MPO) in colon tissue extracts. The data are averages \pm SEM. The 2-sided Wilcoxon rank sum test was performed for analysis. * $P < .05$, ** $P < .01$, *** $P < .001$.

A therapeutic approach consisting of increasing the intraluminal concentration of AMPs to preserve host-microbiota homeostasis and thus prevent intestinal inflammation was proposed.⁴⁵ However, preclinical models based on the enteric delivery of such biological agents were lacking because, among other things, of their proteolytic destruction in the upper digestive tract. The *REG3A*-TG mouse model we used enabled us to deliver a full-length human REG3A protein in the lower digestive tract lumen at sufficient doses to provide clear phenotypic effects in these mice, demonstrating the potential of an approach consisting of administering a large dose of exogenous REG3 to an organism already provided with an endogenous REG3-mediated response to intestinal inflammation.⁴⁶ The phenotypic features of *REG3A*-TG mice include significant changes in gut microbiota composition and a dramatic improvement of host resistance to intestinal inflammation, compared with control mice. *REG3A*-TG mice exposed to DSS exhibited very few signs of colitis, retained a tight mucosal barrier, and achieved complete survival. The inflammatory response and the oxidative stress in the colon epithelium was much reduced in *REG3A*-TG, compared with WT, mice with DSS-induced colitis. A low level of inflammation and mucosal damage was also found in *REG3A*-TG mice with

TNBS-induced colitis. The decrease in ROS levels in the fecal microbiota of *REG3A*-TG compared with control mice on DSS exposure and the increase of survival to ambient-air exposure of highly oxygen-sensitive bacteria cultured in the presence of rcREG3A demonstrate an antioxidant activity of hREG3A on prokaryotic cells that might modify host-microbiota interplay.

The microbial changes exhibited by *REG3A*-TG mice in homeostatic and inflammatory conditions mainly concerned an enrichment of Clostridiales (Ruminococcaceae, Lachnospiraceae) and a depletion of Bacteroidetes (Prevotellaceae). Mice heterozygous for *REG3A* that harbored a WT maternal microbiota at birth progressively acquired a gut microbiota composition close to that of *REG3A* homozygous TG mice, demonstrating the capability of hREG3A to shape the gut microbiota, and then exhibited a resistance to colitis similar to that of homozygous mice. The transfer of a hREG3A-shaped microbiota to WT mice by cohousing or feces gavage resulted in a less-severe disease, a reduced LPS-induced endotoxemia, and a higher survival to DSS exposure than in control groups, establishing the beneficial nature of the hREG3A-shifted microbiota composition. The phenotypic resistance was not fully transmitted by transfer experiments, suggesting that hREG3A acted also by other

ways, including direct mucosal effect, in *REG3A*-TG mice. Repeated intravenous administration of rcREG3A were ineffective, invalidating the hypothesis of a systemic anti-colitogenic effect, whereas rectal administrations of rcREG3A helped to preserve gut barrier integrity during induced colitis in control mice.

Thus, hREG3A provides protection against inflammation and oxidative stress for both the intestinal epithelium and the commensal communities that form the gut microbiota. Future studies will be necessary to determine the sites involved in the ROS scavenging activity of hREG3A. Whether murine *Reg3b* and *Reg3g* encode proteins that carry similar antioxidant properties also needs to be determined.

Regarding the role of hREG3A in the host-gut microbiota interaction, we suggest that the broad-spectrum antioxidant activity of hREG3A may change the balance between different bacterial communities with different oxygen tolerances. In our mouse model, some highly oxygen-sensitive commensal bacteria could be responsive to an exogenous antioxidant, such as hREG3A, giving them a selective advantage over aerotolerant anaerobic ones (ie, those developing an effective adaptive response to oxygen toxicity). In this hypothesis, hREG3A would shape the gut microbiota in the steady state through its antioxidant activity against the environmental stressors existing in the healthy gut and continue to exert this effect under inflammation and oxidative stress. This view is supported by the fact that hREG3A enhanced the growth of some highly oxygen-sensitive Clostridiales commensals. An enrichment of such symbionts may trigger a virtuous process by improving gut barrier function and reducing ROS production, which feeds back into benefiting symbionts. Conversely, an increase in gram-negative commensal bacteria may trigger macrophage activation, increase ROS production, and amplify mucosal injuries and dysbiosis in favor of aerotolerant commensals. Our results suggest that the pressure exerted by hREG3A on the gut microbiota triggers such a virtuous shift in composition and functionality.

From a clinical viewpoint, our findings suggest that an increase in intraluminal concentration of hREG3A, for instance via a colon-targeted delivery method, may be a valuable approach to attenuate intestinal inflammation. Regarding the potential benefits to patients, such an approach would be a more physiological and nontoxic strategy for the treatment of inflammatory outbreaks than the available therapies. Moreover, it might be most successful in the early stages of the inflammatory process and could therefore be useful for the maintenance of medically or surgically induced remission and even the prevention of IBD in high-risk individuals.

Supplementary Material

Note: To access the supplementary material accompanying this article, visit the online version of *Gastroenterology* at www.gastrojournal.org, and at <https://doi.org/10.1053/j.gastro.2017.11.003>.

References

1. Klag T, Stange EF, Wehkamp J. Defective antibacterial barrier in inflammatory bowel disease. *Dig Dis* 2013; 31:310–316.
2. Gevers D, Kugathasan S, Denson LA, et al. The treatment-naive microbiome in new-onset Crohn's disease. *Cell Host Microbe* 2014;15:382–392.
3. Sartor RB, Wu GD. Roles for intestinal bacteria, viruses, and fungi in pathogenesis of inflammatory bowel diseases and therapeutic approaches. *Gastroenterology* 2017;152:327–339.e4.
4. Winter SE, Lopez CA, Bäumlner AJ. The dynamics of gut-associated microbial communities during inflammation. *EMBO Rep* 2013;14:319–327.
5. Albenberg L, Esipova TV, Judge CP, et al. Correlation between intraluminal oxygen gradient and radial partitioning of intestinal microbiota. *Gastroenterology* 2014; 147:1055–1063.e8.
6. Ballal SA, Veiga P, Fenn K, et al. Host lysozyme-mediated lysis of *Lactococcus lactis* facilitates delivery of colitis-attenuating superoxide dismutase to inflamed colons. *Proc Natl Acad Sci U S A* 2015; 112:7803–7808.
7. Dubourg G, Lagier J-C, Hüe S, et al. Gut microbiota associated with HIV infection is significantly enriched in bacteria tolerant to oxygen. *BMJ Open Gastroenterol* 2016;3:e000080.
8. Zasloff M. Antimicrobial peptides of multicellular organisms. *Nature* 2002;415:389–395.
9. Vaishnav S, Yamamoto M, Severson KM, et al. The antibacterial lectin RegIII γ promotes the spatial segregation of microbiota and host in the intestine. *Science* 2011;334:255–258.
10. Salzman NH, Hung K, Haribhai D, et al. Enteric defensins are essential regulators of intestinal microbial ecology. *Nat Immunol* 2010;11:76–83.
11. Dupont A, Kacanis Y, Yang I, et al. Intestinal mucus affinity and biological activity of an orally administered antibacterial and anti-inflammatory peptide. *Gut* 2015; 64:222–232.
12. Wang G. Human antimicrobial peptides and proteins. *Pharmaceuticals (Basel)* 2014;7:545–594.
13. Cullen TW, Schofield WB, Barry NA, et al. Gut microbiota. Antimicrobial peptide resistance mediates resilience of prominent gut commensals during inflammation. *Science* 2015;347:170–175.
14. Pang X, Xiao X, Liu Y, et al. Mosquito C-type lectins maintain gut microbiome homeostasis. *Nat Microbiol* 2016;1:16023.
15. Juneja P, Lazzaro BP. Population genetics of insect immune responses. In: Rolff J, Reynolds S, eds. *Insect infection and immunity*. Oxford, UK: Oxford University Press, 2009:206–224.
16. Goldman MJ, Anderson GM, Stolzenberg ED, et al. Human beta-defensin-1 is a salt-sensitive antibiotic in lung that is inactivated in cystic fibrosis. *Cell* 1997;88:553–560.
17. Schroeder BO, Wu Z, Nuding S, et al. Reduction of disulphide bonds unmasks potent antimicrobial activity of human β -defensin 1. *Nature* 2011;469:419–423.

18. Abou Alaiwa MH, Reznikov LR, Gansemer ND, et al. pH modulates the activity and synergism of the airway surface liquid antimicrobials β -defensin-3 and LL-37. *Proc Natl Acad Sci U S A* 2014;111:18703–18708.
19. Moniaux N, Song H, Darnaud M, et al. Human hepatocarcinoma-intestine-pancreas/pancreatitis-associated protein cures fas-induced acute liver failure in mice by attenuating free-radical damage in injured livers. *Hepatology* 2011;53:618–627.
20. Moniaux N, Darnaud M, Garbin K, et al. The Reg3 α (HIP/PAP) lectin suppresses extracellular oxidative stress in a murine model of acute liver failure. *PLoS ONE* 2015; 10:e0125584.
21. Lieu H-T, Batteux F, Simon M-T, et al. HIP/PAP accelerates liver regeneration and protects against acetaminophen injury in mice. *Hepatology* 2005;42:618–626.
22. Lieu H-T, Simon M-T, Nguyen-Khoa T, et al. Reg2 inactivation increases sensitivity to Fas hepatotoxicity and delays liver regeneration post-hepatectomy in mice. *Hepatology* 2006;44:1452–1464.
23. Lai Y, Li D, Li C, et al. The antimicrobial protein REG3A regulates keratinocyte proliferation and differentiation after skin injury. *Immunity* 2012;37:74–84.
24. Lv Y, Yang X, Huo Y, et al. Adenovirus-mediated hepatocarcinoma-intestine-pancreas/pancreatitis-associated protein suppresses dextran sulfate sodium-induced acute ulcerative colitis in rats. *Inflamm Bowel Dis* 2012;18:1950–1960.
25. **Haldipur P, Dupuis N**, Degos V, et al. HIP/PAP prevents excitotoxic neuronal death and promotes plasticity. *Ann Clin Transl Neurol* 2014;1:739–754.
26. **Cash HL, Whitham CV**, Behrendt CL, et al. Symbiotic bacteria direct expression of an intestinal bactericidal lectin. *Science* 2006;313:1126–1130.
27. **Stelter C, Käppeli R**, König C, et al. Salmonella-induced mucosal lectin RegIII β kills competing gut microbiota. *PLoS ONE* 2011;6:e20749.
28. **Ampting MTJ van, Loonen LMP**, Schonewille AJ, et al. Intestinally secreted C-type lectin Reg3b attenuates salmonellosis but not listeriosis in mice. *Infect Immun* 2012;80:1115–1120.
29. Miki T, Holst O, Hardt W-D. The bactericidal activity of the C-type lectin RegIII β against Gram-negative bacteria involves binding to lipid A. *J Biol Chem* 2012;287: 34844–34855.
30. Medveczky P, Szmola R, Sahin-Tóth M. Proteolytic activation of human pancreatitis-associated protein is required for peptidoglycan binding and bacterial aggregation. *Biochem J* 2009;420:335–343.
31. Loonen LMP, Stolte EH, Jaklofsky MTJ, et al. REG3 γ -deficient mice have altered mucus distribution and increased mucosal inflammatory responses to the microbiota and enteric pathogens in the ileum. *Mucosal Immunol* 2014;7:939–947.
32. Simon M-T, Pauloin A, Normand G, et al. HIP/PAP stimulates liver regeneration after partial hepatectomy and combines mitogenic and anti-apoptotic functions through the PKA signaling pathway. *FASEB J* 2003;17:1441–1450.
33. Bus JS, Gibson JE. Paraquat: model for oxidant-initiated toxicity. *Environ Health Perspect* 1984;55:37–46.
34. Ubeda C, Lipuma L, Gobourne A, et al. Familial transmission rather than defective innate immunity shapes the distinct intestinal microbiota of TLR-deficient mice. *J Exp Med* 2012;209:1445–1456.
35. HSP de Souza, Fiocchi C. Immunopathogenesis of IBD: current state of the art. *Nat Rev Gastroenterol Hepatol* 2016;13:13–27.
36. Willing BP, Dicksved J, Halfvarson J, et al. A pyrosequencing study in twins shows that gastrointestinal microbial profiles vary with inflammatory bowel disease phenotypes. *Gastroenterology* 2010;139: 1844–1854.e1.
37. **Quévrain E, Maubert MA, Michon C**, et al. Identification of an anti-inflammatory protein from *Faecalibacterium prausnitzii*, a commensal bacterium deficient in Crohn's disease. *Gut* 2016;65:415–425.
38. Abbeele P Van den, Belzer C, Goossens M, et al. Butyrate-producing *Clostridium* cluster XIVa species specifically colonize mucins in an in vitro gut model. *ISME J* 2013;7:949–961.
39. Duncan SH, Aminov RI, Scott KP, et al. Proposal of *Roseburia faecis* sp. nov., *Roseburia hominis* sp. nov. and *Roseburia inulinivorans* sp. nov., based on isolates from human faeces. *Int J Syst Evol Microbiol* 2006; 56:2437–2441.
40. Khan MT, Duncan SH, Stams AJM, et al. The gut anaerobe *Faecalibacterium prausnitzii* uses an extracellular electron shuttle to grow at oxic-anoxic interphases. *ISME J* 2012;6:1578–1585.
41. **Elinav E, Strowig T**, Kau AL, et al. NLRP6 inflammasome regulates colonic microbial ecology and risk for colitis. *Cell* 2011;145:745–757.
42. Bloom SM, Bijanki VN, Nava GM, et al. Commensal *Bacteroides* species induce colitis in host-genotype-specific fashion in a mouse model of inflammatory bowel disease. *Cell Host Microbe* 2011;9:390–403.
43. Cash HL, Whitham CV, Hooper LV. Refolding, purification, and characterization of human and murine RegIII proteins expressed in *Escherichia coli*. *Protein Expr Purif* 2006;48:151–159.
44. Wirtz S, Popp V, Kindermann M, et al. Chemically induced mouse models of acute and chronic intestinal inflammation. *Nat Protoc* 2017;12:1295–1309.
45. Wehkamp J, Koslowski M, Wang G, et al. Barrier dysfunction due to distinct defensin deficiencies in small intestinal and colonic Crohn's disease. *Mucosal Immunol* 2008;1(Suppl 1):S67–S74.
46. Ogawa H, Fukushima K, Naito H, et al. Increased expression of HIP/PAP and regenerating gene III in human inflammatory bowel disease and a murine bacterial reconstitution model. *Inflamm Bowel Dis* 2003; 9:162–170.

Author names in bold designate shared co-first authorship.

Received January 18, 2017. Accepted November 6, 2017.

Reprint requests

Address requests for reprints to: Jamila Faivre, MD, PhD, INSERM U1193, University Paris-Saclay, Paul-Brousse Hospital, Hepatobiliary Centre, 14 Av. Paul Vaillant-Couturier, Villejuif 94800, France. e-mail: jamila.faivre@inserm.fr; fax: +3314559026.

Acknowledgments

We warmly thank Dr H. Blottière, Professor F. Carbonnel, Professor J.F. Colombel, and Dr P. Langella for fruitful discussions. For experimental assistance, we thank R. Duchateau, Dr C. Martin, Dr K. Lipson (animal care), F. Levenez (gnotobiology, 16S DNA extraction), L. Calvo (16S rDNA libraries), C. Bridonneau (anaerobic bacterial strains), Dr P. Le Baccon (fluorescence microscopy), P. Duchambon (recombinant proteins), the Alfact Innovation Company (ALF5755 recombinant protein), the IGBMC Platform (microarray), the CLNS@Sapienza genomics Platform (sequencing), and the INRA GenoToul Bioinformatics Facility (computing and storage resources).

Jinzi Zheng's present address: Institute of Biomaterials and Biomedical Engineering, University of Toronto, Ontario M5G 1L7, Canada.

Conflicts of interest

The authors disclose no conflicts.

Funding

This work was supported by grants from the Fondation ARC pour la Recherche sur le Cancer (PJA 20111203952, PJA 20131200221, and PJA 20141202048 to J.F.; PJA 20111203952 to N.M.). Sandrine Augui was funded by an Association pour la Recherche sur le Cancer Fellowship (R12036LL). Jamila Faivre was supported by the European Union's Seventh Framework Programme (FP7) under grant agreement No. 259743 (MODHEP consortium), the Institut National du Cancer, the OSEO-BPI Programme d'Investissements d'Avenir (IMODI and HECAM consortiums; R14035LB and R15065LH, respectively).

Supplementary Methods

Animal Studies

Animal studies were performed in compliance with the institutional and European Union guidelines for laboratory animal care and approved by the Ethics Committee of CE2A-03 CNRS-Orléans (Accreditation N°01417.01). The number of *Mus musculus* mice used was in compliance with institutional ethical rules and consistent with common practice in the fields of microbiota analysis and experimental colitis. Conventional mice were produced and housed in the CNRS SEAT and Institut André Lwoff animal care facilities (Université Paris-Sud, Villejuif). Germ-free mice were housed at the Anaxem platform of the Micalis Institute (INRA, Jouy-En-Josas). All the conventionally bred mouse groups were homogeneous in terms of age (10–12 weeks), weight (25 g), sex (50% male and 50% female), and environmental factors. All the *REG3A*-TG mice had circulating hREG3A levels within the 200 to 600 ng/mL range. None was excluded from the study. WT and *REG3A*-TG mice had the same C57BL/6N genetic background. They were not littermates. WT female mice were crossed with *REG3A* homozygous males to generate heterozygous pups harboring the maternal microbiota at birth. For the cohousing experiments, 3-week-old weaned *REG3A*-TG mice were cohoused randomly with age-matched WT mice at a 1:1 ratio for 8 weeks. Some of these mice were exposed to DSS, and others were used for tissue analysis at the end of the cohousing period. For the feces transfer experiments, male germ-free C57BL/6 mice were housed in sterile isolators. Their germ-free status was checked weekly using microbiological assays on feces and drinking water. At the age of 10 weeks, the germ-free mice underwent 2 gastric gavages at 48-hour intervals, using 0.5 mL of inoculum prepared from conventional mice fecal microbiota diluted 1/100. Inocula consisted of pooled feces from 8 TG or 8 WT mice. To induce colitis, mice were fed with a 3% 40-kDa DSS solution (TdB Consultancy AB) added to their drinking water for 5 days (solution changed every day). The animals were then fed with tap water for 7 additional days. Weight loss, stool consistency, and bleeding were evaluated daily. Scores are defined as follows: stool consistency: 0 (normal), 1 (soft), 2 (very soft), 3 (diarrhea); stool bleeding: 0 (normal), 1 (red), 2 (dark red), 3 (gross bleeding). For colitis induction by TNBS (Sigma-Aldrich), overnight-fasted mice were anesthetized for 90 minutes and received a single intrarectal administration of TNBS (40 μ L, 150 mg/kg) dissolved in a 1:1 mixture of 0.9% NaCl with 100% ethanol. Control mice received a 1:1 mixture of 0.9% NaCl with 100% ethanol. The WT mice that were administered the recombinant hREG3A protein received an intrarectal injection of 100 μ g rcREG3A on the day before and on the day of TNBS administration. Macroscopic examination, histological analysis, and quantitative polymerase chain reaction (qPCR) were performed 2 days after TNBS administration. The different mouse groups (WT or TG, single-housed or cohoused, conventionally fed or germ-free) were used exhaustively.

Composition of the Microbiota

DNA pyrosequencing of the V3-V4 hypervariable region of 16S rRNA gene was performed using the Illumina MiSeq instrument. The sequences thus generated were pre-processed using the mothur pipeline and then clustered into operational taxonomic units based on 97% of similarity. Using the RDP Classifier, we assigned operational taxonomic units to taxa (genus-level) with a confidence threshold of 80%. RDP release 11 was used as the reference database. PCA was performed based on bacterial family and genera compositions using the R packages *ade4* and *FactoMiner*. Families representing more than 0.5% of the total bacterial population were taken into account. The robustness of each clustering result was assessed using a Monte-Carlo rank test ($B = 999$ repetitions, $P < .05$). Differences between groups were analyzed using a nonparametric Wilcoxon rank-sum test. All the relevant data can be found in the text, except for the DNA sequence reads, which are available from the Sequence Read Archive (accession numbers pending) or by contacting the corresponding author.

Bacterial Strains, Culture Conditions, and Flow Cytometry

Gram-positive *Enterococcus faecalis* ATCC-19433 were grown at 37°C under shaking in BHI (BD Bacto Brain Heart Infusion; Thermo Fisher Scientific, France) broth overnight and then in LB (Luria-Bertani; Becton Dickinson, Franklin Lakes, NJ). To induce peroxide stress on *E faecalis*, 5.10^6 bacteria per mL were incubated at 37°C with 200 mM paraquat (1,1'-dimethyl-4,4'-bipyridinium dichloride; Sigma-Aldrich) and 10 μ M of rcREG3A protein or equivalent volume of buffer. The reagents were added to the culture during the log phase. Colony-forming units (CFUs) were counted after plating serial dilutions on LB agar plates incubated at 37°C overnight. All cultures were performed in quadruplicate during 3 independent experiments. Intracellular ROS levels and cell viability were determined by flow cytometry with 2',7'-dichlorofluorescein diacetate (H₂-DCFDA; Life Technologies) and propidium iodide (Sigma-Aldrich) in *E faecalis* cultures incubated with paraquat alone or paraquat supplemented with 10 μ M rcREG3A for 8 hours. H₂-DCFDA was dissolved in dimethyl sulfoxide (Sigma-Aldrich) to 10 mM and added at a final concentration of 10 μ M. After incubating *E faecalis* cultures for 30 minutes in the dark at 37°C, the cells were pelleted, washed twice with phosphate-buffered saline (PBS), suspended in 1 mL PBS supplemented with 1 μ g/mL propidium iodide, and processed in a BD Accuri C6 flow cytometer (Becton Dickinson). For the measurements of bacterial ROS levels in fecal microbiota, fresh feces were suspended in cold PBS and centrifuged twice at 447 g for 5 minutes at 4°C. The supernatant was incubated with PBS containing 25 μ M H₂-DCFDA for 15 minutes and then centrifuged at 2795 g for 5 minutes. The resulting pellet was suspended in cold PBS and processed in the flow cytometer. Analysis of the flow data was performed using Flow Jo software (Ashland, OR). *Faecalibacterium prausnitzii* A2-165 (DSM17677) and *Roseburia intestinalis* L1-82 (DSM14610T) were grown under strict anaerobic conditions at 37°C for 24 hours in LYHBHI medium (BHI broth supplemented with 0.5% yeast extract and

5 mg/L hemin) supplemented with 1 mg/mL maltose, 1 mg/mL cellobiose, and 0.5 mg/mL cysteine-HCl. Anaerobic growth of *F. prausnitzii* and *R. intestinalis* was performed in the presence of 5 μ M of rcREG3A for 7 or 24 hours, respectively, and followed by a 5-minute exposure to ambient air. Bacterial growth was assessed by CFU counting on agar plates. CFU numbers were normalized to the average CFU number measured in control cultures (buffer). Protein extracts from *F. prausnitzii* grown for 2 or 24 hours with rcREG3A or buffer were subjected to sodium dodecyl sulfate–polyacrylamide gel electrophoresis. Each experiment was performed in quadruplicate during 3 independent experiments. Wet mounts were observed using a Deltavision optical microscope (Applied Precision Inc, Issaquah, WA) with a $\times 63$ objective lens.

Recombinant REG3A Proteins

Two batches of recombinant proteins were used; one (ALF5755) supplied by the Alfact Innovation Company (Paris, France) and the other made in our laboratory. We subcloned the coding sequence corresponding to the secreted form of hREG3A within pET28-N-HIS-SUMO (Novagen, Molsheim, France). The resulting construct was verified by sequencing and then transformed into an engineered *Escherichia coli* BL21 (DE3) strain co-expressing the sulfhydryl oxidase, Erv1p, and the disulphide isomerase, DsbC. These modifications enabled the efficient production of natively folded hREG3A in the cytoplasm. The hREG3A proteins were produced in a 7L Infors-Labfors fermenter (Infors Ltd, Massy, France) at 20°C and pH 6.8 \pm 0.1 for 16 hours. These cells were then pelleted and lysed using a one-shot desintegrator (CellD, Roquemaure, France) at 1.5 kbar. The proteins were purified from the supernatant using Ni-NTA resin (Macherey Nagel, Duren, Germany), cleaved with a home-made SUMO protease. The His-tag and Sumo protease were removed from the protein suspension by a Ni-NTA resin. The resulting supernatant was dialyzed against 50 mM phosphate buffer pH 7.4.

Enzyme-Linked Immunosorbent Assays

The serum concentrations of Reg3g, hREG3A, LPS, and soluble CD14 were measured using the E94676Mu (Usnc Life Science Inc, Houston, TX), PancrePAP (Dynabio, Lyon, France), LAL chromogenic endpoint (Hycult biotech, Plymouth Meeting, PA) and One Step ELISA (BioMetec, Greifswald, Germany) kits, respectively, according to the manufacturer's instructions. The myeloperoxidase concentration in colon tissues homogenates was determined using the mouse MPO ELISA kit (Hycult biotech).

Histological Analysis

For each mouse studied, 2 samples from the distal and proximal colon were fixed in 4% paraformaldehyde acid and then embedded in paraffin; 4- μ m-thick sections were deparaffinized in xylene for 5 minutes and rehydrated for 5 minutes in 100%, 90%, and 70% ethanol successively. They were then stained with hematoxylin/eosin/Alcian blue, randomly sorted, and scored in a blind manner by an expert in pathology. The score used for DSS-induced colitis was as follows: Grade 0, normal mucosa; Grade 1, infiltration of

inflammatory cells; Grade 2, crypt abscesses and erosion; and Grade 3, destruction of epithelial cells (ulceration and loss of Goblet cells). The number of sections analyzed per colon sample ranged from 2 to 6. The Ameho score used for TNBS-induced colitis reads: Score 0, no lesion; Score 1, mild mucosal or submucosal inflammatory infiltrate with edema, punctuate mucosal erosions, muscularis mucosae intact; Score 2, score 1 changes involving 50% of the specimen; Score 3, prominent inflammatory infiltrate with deeper areas of ulceration extending through the muscularis mucosae into the submucosa; Score 4, score 3 changes involving 50% of the specimen; Score 5, extensive ulceration with coagulative necrosis extending deeply into the muscularis mucosae; and Score 6, score 5 changes involving 50% of the specimen.

Immunohistochemistry

Formalin-fixed, paraffin-embedded colon sections (4 μ m) were de-waxed in xylene and rehydrated through graded alcohols. Tissue sections were pressure cooked in 10 mM citrate buffer pH 6 for 5 minutes, incubated with 3% H₂O₂ for 20 minutes to block endogenous peroxidase, and then incubated with a laboratory-made purified rabbit polyclonal anti-hREG3A antibody.¹ Secondary anti-rabbit immunoglobulin G–horseradish peroxidase (HRP) was used according to the manufacturer's instructions (DAKO, Glostrup, Denmark). The sections were counterstained with Alcian blue (Sigma) before mounting the coverslips.

Lipid Peroxidation

Malondialdehyde was dosed using the thiobarbituric acid method as previously described.¹ A standard curve was prepared using malondialdehyde tetrabutylammonium salt (Sigma-Aldrich, Lyon, France). The results were normalized in relation to the total protein content.

In Situ Hybridization and Immunofluorescence

Unwashed segments of colon and mesenteric lymph nodes were fixed in methanol-Carnoy mixture, followed by embedding in paraffin. Paraffin sections (3 to 5 μ m) were de-waxed and washed in 100% ethanol. Fluorescence in situ hybridization (FISH) was performed as previously described.² The oligonucleotide probes used are EUB338 and univ1390 for universal 16S RNA (see the probeBase online resource). Bacterial translocation levels in mesenteric lymph nodes were determined on FISH images in at least 1 to 2 lymph nodes per mouse and 3 sections per node. Anti-Mucin2 antibody (H300, sc-15334; Santa Cruz Biotechnology, Heidelberg, Germany) was used at a dilution of 1:100 in 4% goat serum. The Muc2 signal was detected using a goat anti-rabbit immunoglobulin G–Alexa 598 (A11036; Molecular Probes, Eugene, OR). The tissues were counterstained with 4',6-diamidino-2-phenylindole, and fluorescent images were acquired using a Deltavision real-time microscope piloted by SoftWorx software (Applied Precision, GE Healthcare, Little Chalfont, UK), with a $\times 40/1.4$ NA objective (Olympus, Tokyo, Japan) and a charge-coupled device CoolSNAP HQ2 camera (Photometrics, Tucson, AZ).

Transcriptomics, qPCR

RNAs were purified from colon tissues using the mir-Vana miRNA isolation kit (Ambion, Austin, TX). RNA quality was evaluated with the Agilent 2100 bioanalyzer (Agilent Technologies, Santa Clara, CA). Samples with an RNA integrity number higher than 7 were processed for transcriptomic analysis. Biotinylated single strand cDNA targets were prepared from 200 ng total RNA using the Ambion WT Expression Kit and the Affymetrix (Santa Clara, CA) GeneChip WT Terminal Labeling Kit, according to the manufacturer's instructions. A total of 1.9 μg of cDNAs were hybridized for 16 hours at 45°C on GeneChip Mouse Gene 1.0 ST arrays (Affymetrix) interrogating 28,853 genes represented by approximately 27 probes spread along the full length of the gene. The chips were washed and stained in the GeneChip Fluidics Station 450, and scanned with the GeneChip Scanner 3000 7G at a resolution of 0.7 μm . CEL files were further processed with Affymetrix Expression Console software version 1.1 to calculate the probe set signal intensities using Robust Multi-array Average algorithms with default settings. Transcriptomic data have been deposited in Gene Expression Omnibus (National Center for Biotechnology Information, Bethesda, MD) under the accession number GSE64932. For qPCR, the sequences of the specific primers used were as follows. Tnf-F: GGGAG TAGACAAGGTACAAC; Tnf-R: TCTCATCAGTTCTATGGCCC. Il1-F: CAACCAACAAGTGATATTCTCCATG; Il1-R: GATCCA CACTCTCCAGCTGCA. Hprt-F: AGGACCTCTCGAAGTGT; Hprt-R: TCAATCCCTGAAGTACTCAT.

Gene Set Enrichment Analysis

Gene set enrichment analysis was performed to explore the gene sets differentially expressed between WT and *REG3A*-TG mice. Gene set enrichment analysis version 2.0 software was downloaded from the Broad Institute (Cambridge, MA) Web site, working with version 4.0 of MsigDB. The most significant gene sets are displayed with their corresponding normalized enrichment scores and nominal *P* values. Medline/PubMed data mining for LPS-endotoxin functionality was performed using LPS and endotoxin as the keywords. A total of 356 genes with a raw *P* value less than .05 were retrieved from 4267 articles. Eighty-five genes were still related to LPS-induced cellular responses after correction of the multitesting error by the false discovery rate. Unsupervised hierarchical clustering (Euclidean distance and complete linkage) was performed using the expression profiles of the 85-gene set.

Immunoblotting

The quantification of hREG3A protein along the gastrointestinal tract of *REG3A*-TG mice was performed using the anti-hREG3A immunoblotting of 50 μg total protein. Immunodetection of the rcREG3A in bacterial cultures was performed by spinning down 200 μL of a bacterial culture previously incubated with rcREG3A or buffer for 2 or 24 hours. The pellet was washed 3 times with PBS supplemented with a protease inhibitor cocktail (eComplete; Roche, Basel, Switzerland), resuspended in 30 μL Laemmli

buffer, and stored at -20°C . After denaturation for 5 minutes at 95°C, the sample extracts were separated on 15% polyacrylamide gel by sodium dodecyl sulfate-polyacrylamide gel electrophoresis, and then transferred onto a nitrocellulose membrane for immunoblotting using our anti-hREG3A antibody. Total protein lysates were extracted from mouse colon tissues with RIPA buffer (50 mM Tris-Cl pH 7.4, 150 mM NaCl, 1% NP40, 0.25% sodium deoxycholate, protease inhibitors). To detect O-glycoproteins containing Core 3, 500 ng protein was resolved on 4% to 15% precast polyacrylamide gel (Bio-Rad, Hercules, CA), electro-transferred onto a nitrocellulose membrane, and hybridized with wheat germ agglutinin conjugated with HRP (Sigma-Aldrich).

Dot Blot

Monosaccharides (glucose, mannose) and polysaccharides (LPS, peptidoglycan, mannan, DSS) (Sigma-Aldrich) at 2 doses (30 ng, 150 ng) were spotted onto nitrocellulose membranes and cross-linked to the membrane using UV irradiation. The membranes were washed twice with PBS, and hybridized with 1 $\mu\text{g}/\text{mL}$ of rcREG3A at 37°C for 2 hours. Nonhybridized hREG3A proteins were washed away with TBST (50 mM Tris-Cl pH 7.4, 150 mM NaCl, 0.1% Tween), The membranes were incubated with our anti-hREG3A antibody for 30 minutes at room temperature and then with HRP-conjugated goat anti-rabbit antibody to reveal the hREG3A proteins attached to saccharides.

[^{18}F]FDG Positron Emission Tomography Scan

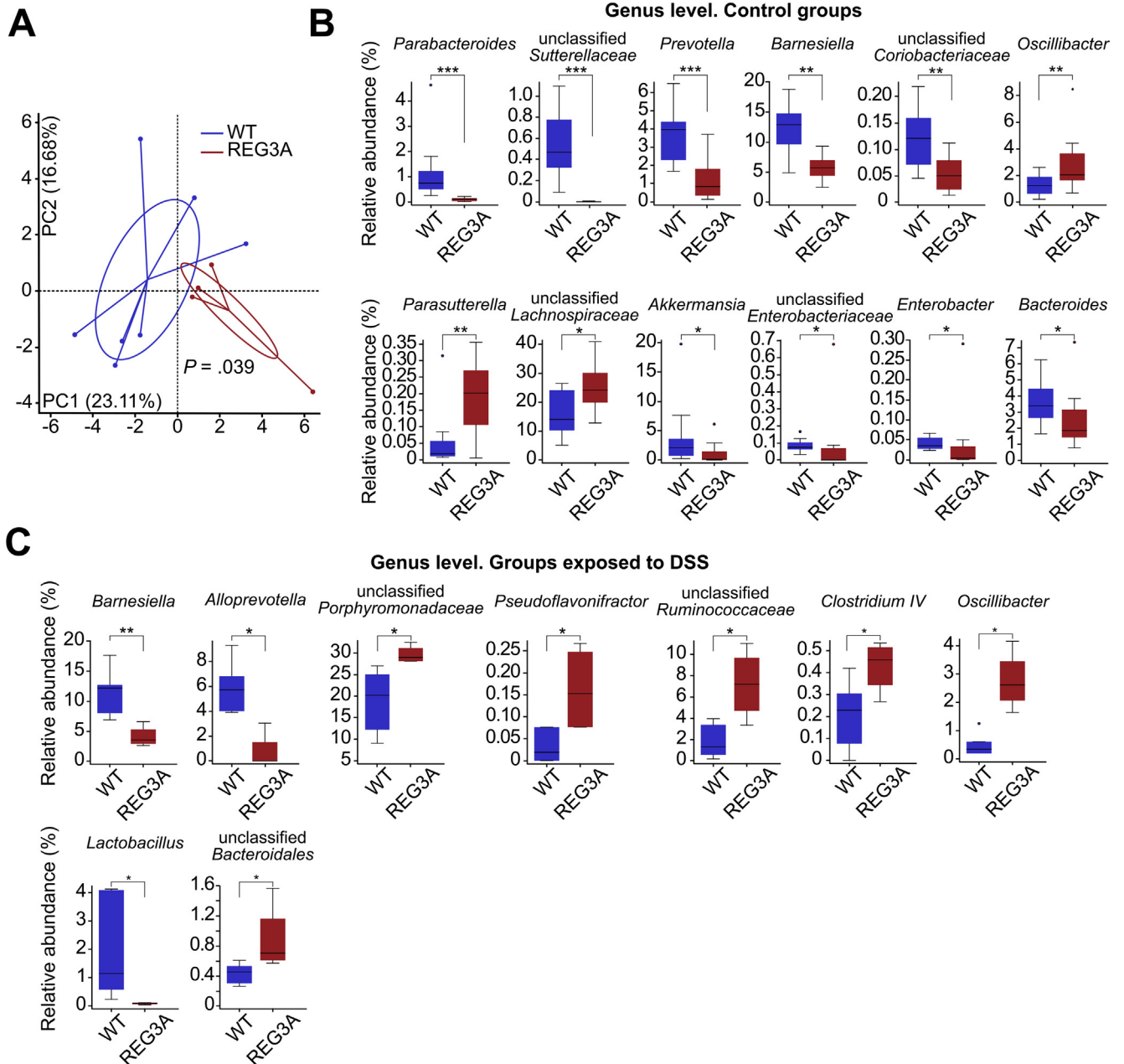
[^{18}F]FDG was purchased from Cyclopharma S.A. (Clermont-Limagne, France). The mice to be imaged were anesthetized with oxygen-isoflurane (2% isoflurane, 0.4 L/min oxygen) and kept at a physiological body temperature on a heating pad. Three male WT and *REG3A*-TG mice were injected intravenously with 10 MBq [^{18}F]FDG in 100 μL PBS on different days of induced colitis. The images were acquired dynamically over 15 minutes as from 1 hour after the radioisotope injection, using a microPET Focus (Siemens, Munich, Germany). The uptake of radioactivity was quantified in regions of interest drawn in the abdominal areas of the reconstructed PET images. For each region of interest, the mean uptake was calculated as the percent-injected dose per gram tissue (%ID/g) assuming a tissue density of 1 g/cm³.

Statistics

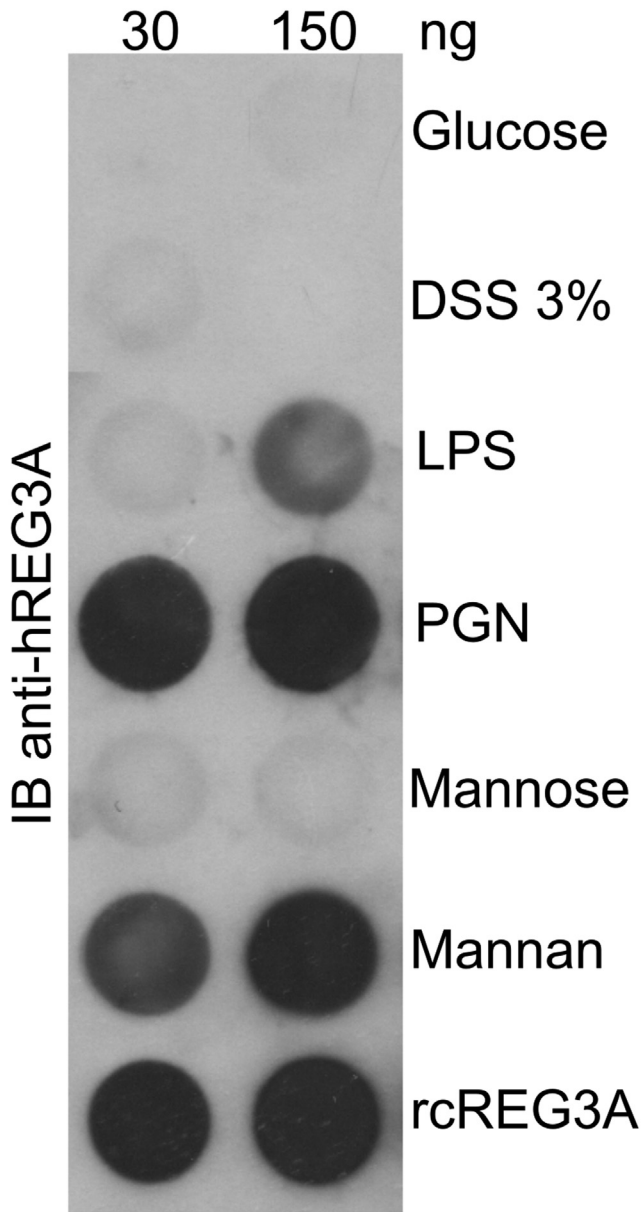
Results are presented as means \pm SEM or box plots. Differences between sample groups were tested using nonparametric Wilcoxon rank sum (2-sided) for all the experiments reported, with the following exceptions: 2-way analysis of variance tests were used for the in vivo quantifications of [^{18}F]FDG and H₂-DCFDA over time; the robustness of PCA clustering was assessed with a Monte-Carlo rank test; the Kaplan-Meier survival analysis with a log-rank test was applied to compare the time course of survival between the groups. *P* values less than .05 were considered to be statistically significant.

Supplementary References

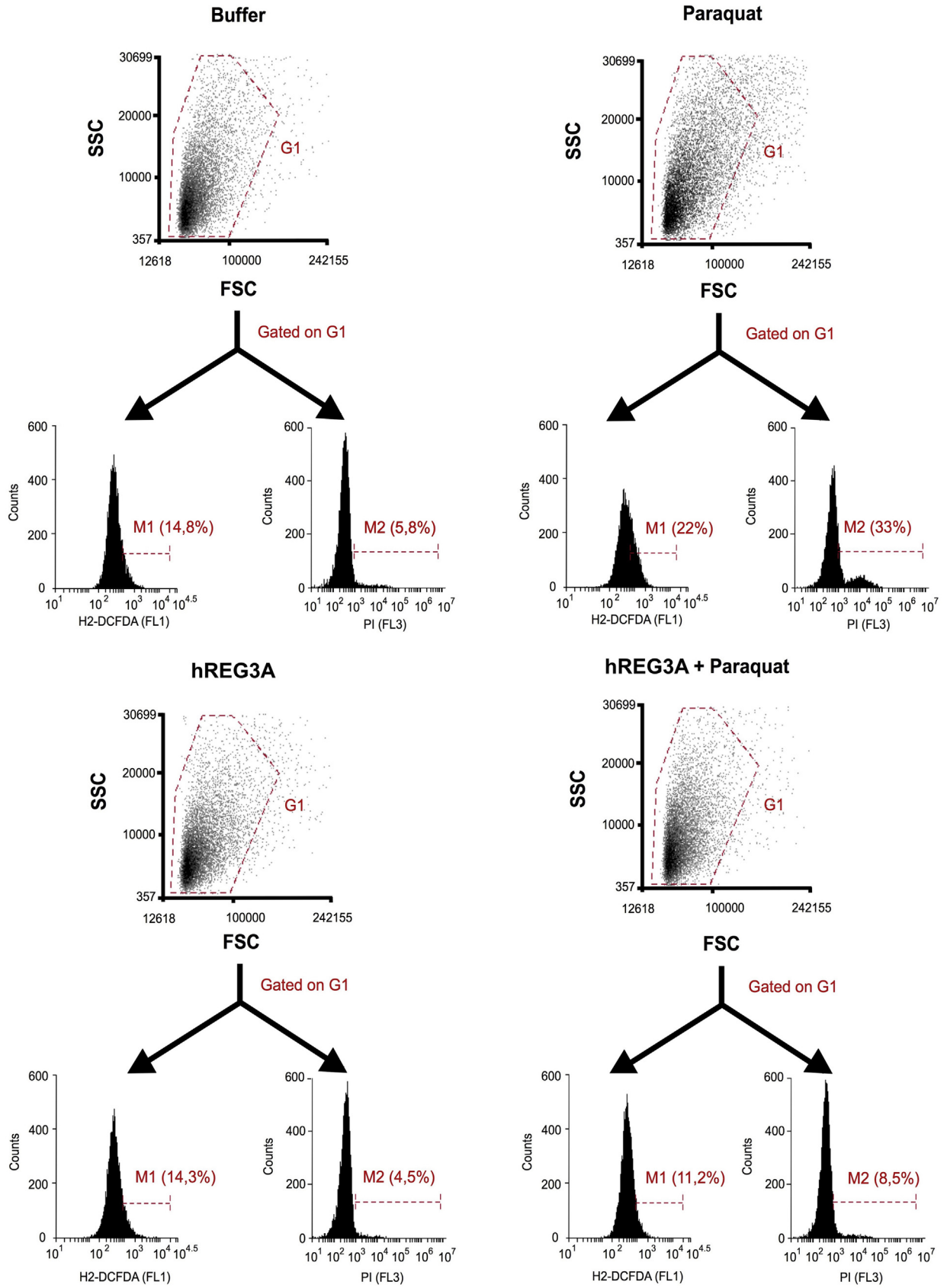
1. Moniaux N, Song H, Darnaud M, et al. Human hepatocarcinoma-intestine-pancreas/pancreatitis-associated protein cures fas-induced acute liver failure in mice by attenuating free-radical damage in injured livers. *Hepatology* 2011;53:618–627.
2. Canny G, Swidsinski A, McCormick BA. Interactions of intestinal epithelial cells with bacteria and immune cells: methods to characterize microflora and functional consequences. *Methods Mol Biol* 2006;341:17–35.

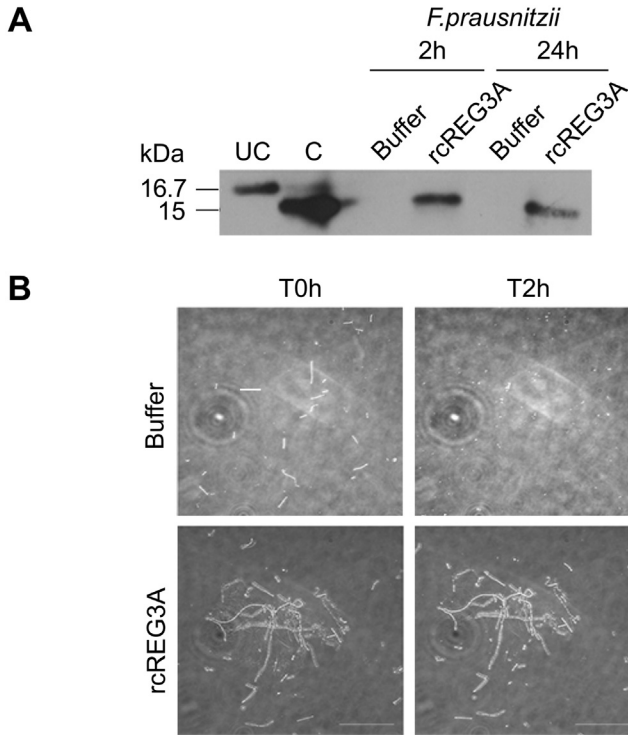


Supplementary Figure 1. Gut microbiota composition under homeostatic and inflammatory conditions in *REG3A*-transgenic mice. (A) PCA plots of bacterial profiles at the family level in *REG3A*-TG ($n = 4$) and WT ($n = 7$) mice on day 12 of induced colitis. $P = .039$ (Monte-Carlo rank test). Each dot represents 1 mouse. (B) and (C) Relative abundances of bacterial genera in (B) the homeostatic (Control groups) and (C) inflammatory (Groups exposed to DSS) states. The data are averages \pm SEM. The Wilcoxon rank-sum test was performed for analysis.

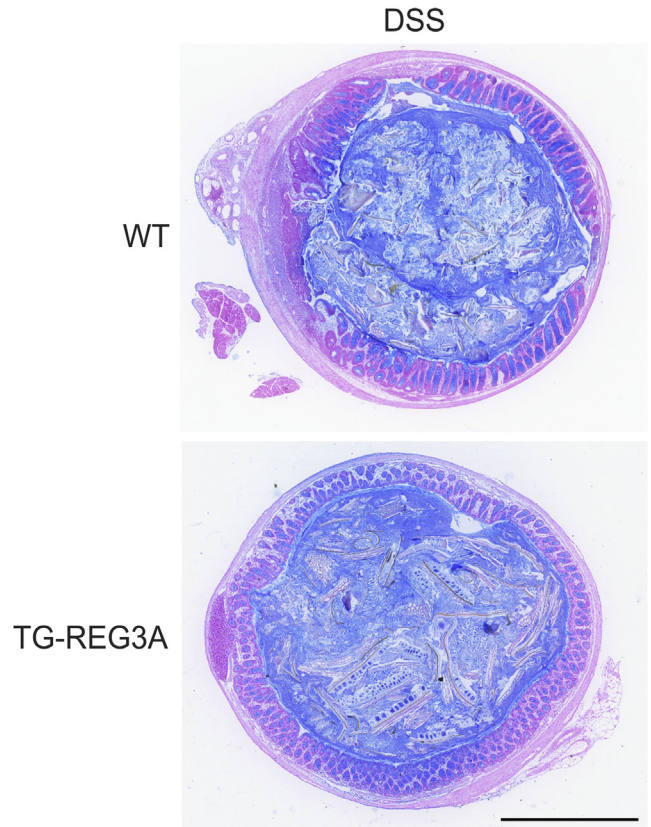


Supplementary Figure 2. The hREG3A lectin does not interact with DSS. Dot blot of hREG3A binding to the indicated immobilized mono- and polysaccharides followed by anti-hREG3A immunoblotting (IB). PGN, peptidoglycans. The lane labeled rcREG3A received no saccharides.



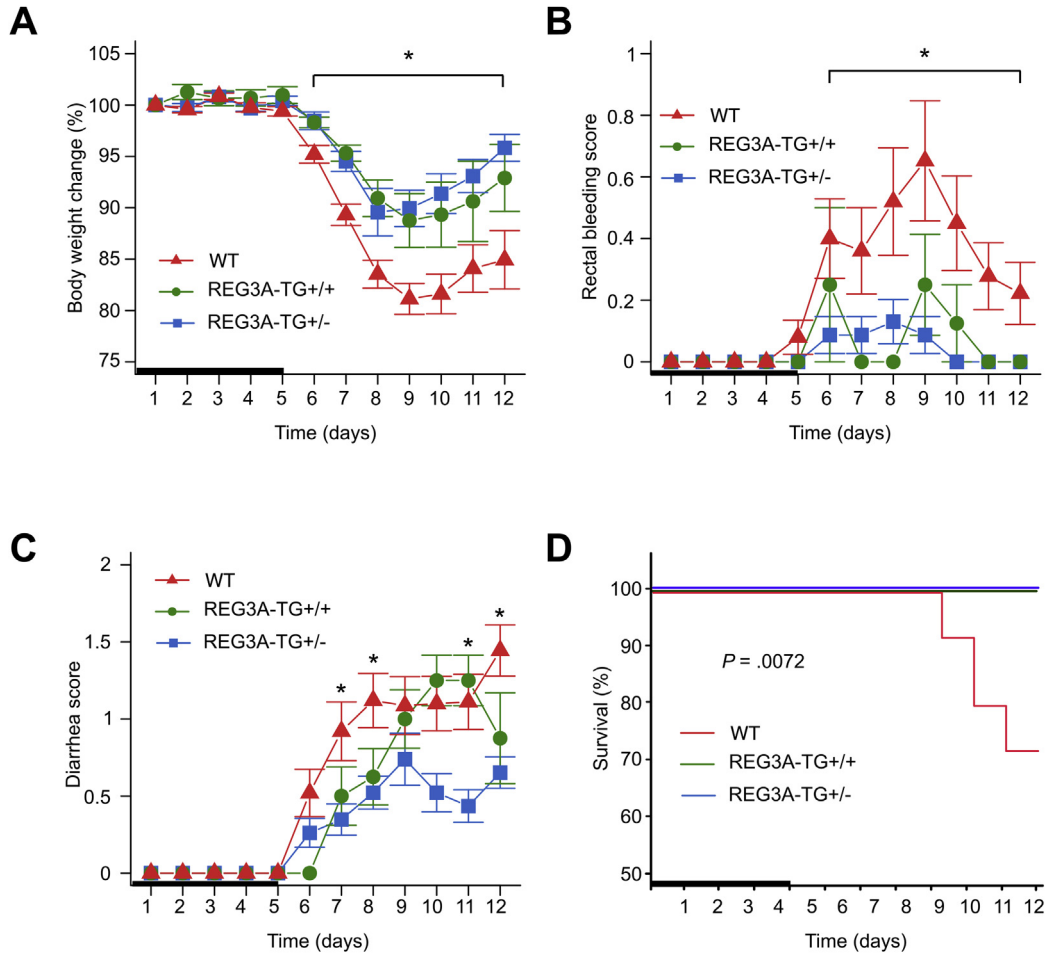


Supplementary Figure 4. hREG3A increases the viability of *F. prausnitzii* exposed to ambient air. (A) Anti-hREG3A immunoblot from *F. prausnitzii* anaerobic cultures incubated with a rcREG3A for 2 or 24 hours. Uncleaved (UC) and cleaved (C) rcREG3A: control signals. (B) Micrographs of slide-mounted *F. prausnitzii* colonies without or with rcREG3A before (T0h) and after (T2h) exposure to ambient air. Scale bar, 20 μ m.



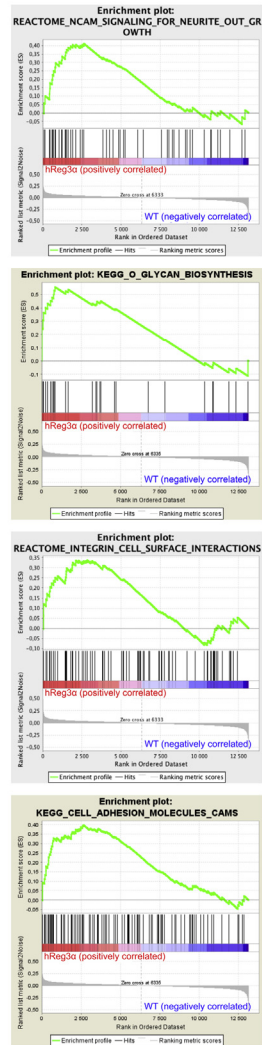
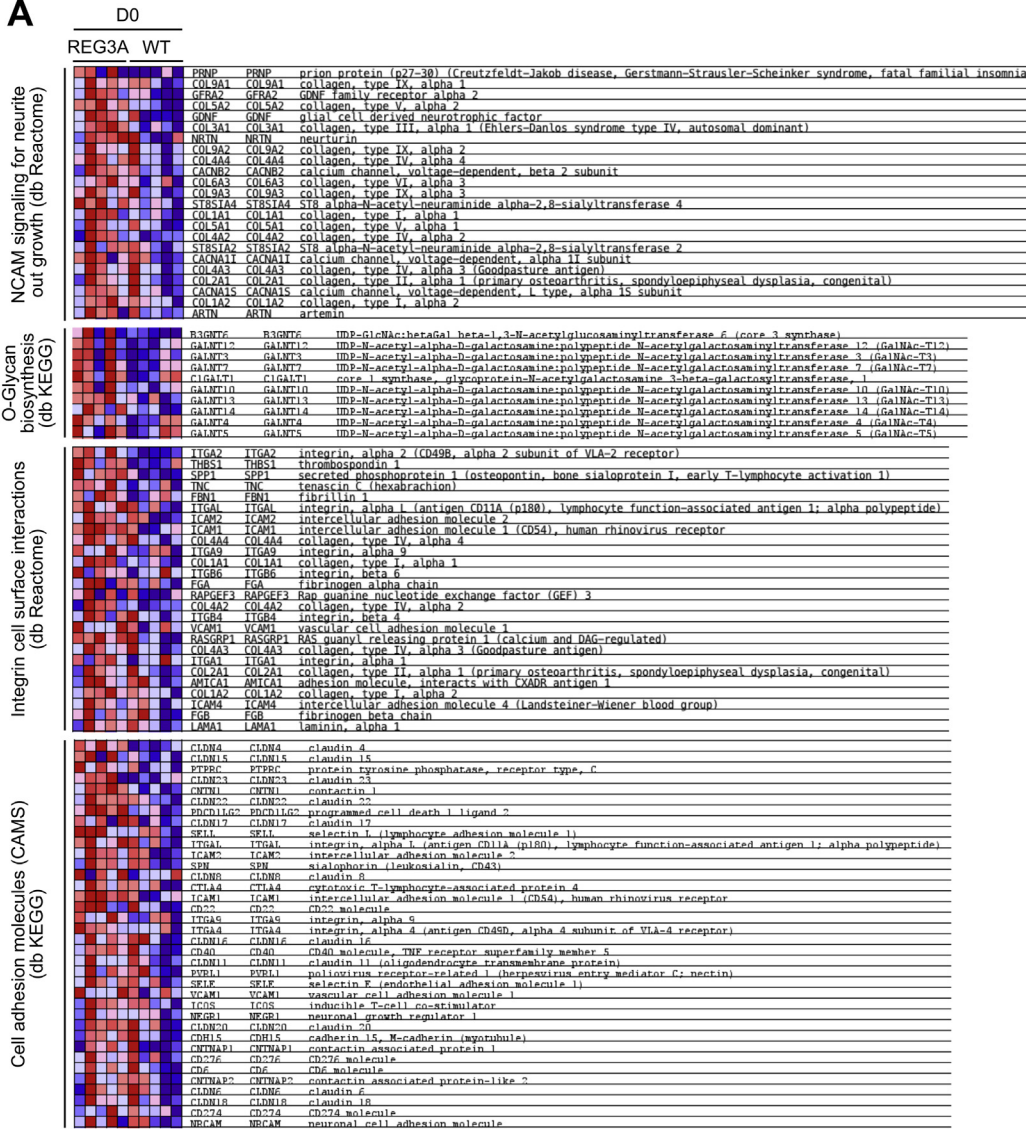
Supplementary Figure 5. Representative colon images stained with hematoxylin, eosin, and Alcian blue at day 12 of DSS-induced colitis in *REG3A*-transgenic (TG-REG3A) and WT mice. Same colon sections as in Figure 3E. Scale bar, 1 mm.

Supplementary Figure 3. Representative flow cytometry plots of cellular ROS levels (H_2 -DCFDA dye; FL1 detector) and cell viability (propidium iodide [PI]; FL3 detector) in *E. faecalis* cultures exposed to paraquat and hREG3A. Gate G1 (alive cell population) representing 90% of the total cell population was defined in the forward (FSC) and side (SSC) scatter light plots in the cultures incubated with buffer. Gate M1 was set to include the 15% most strongly FL1 fluorescent cells and Gate M2 the 5% most strongly FL3 fluorescent cells in the buffer condition. The same G1, M1, and M2 gates were used in the analysis of cultures exposed to paraquat and hREG3A.

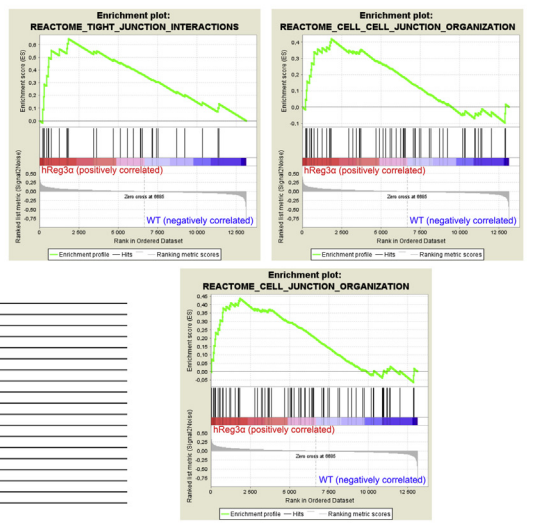
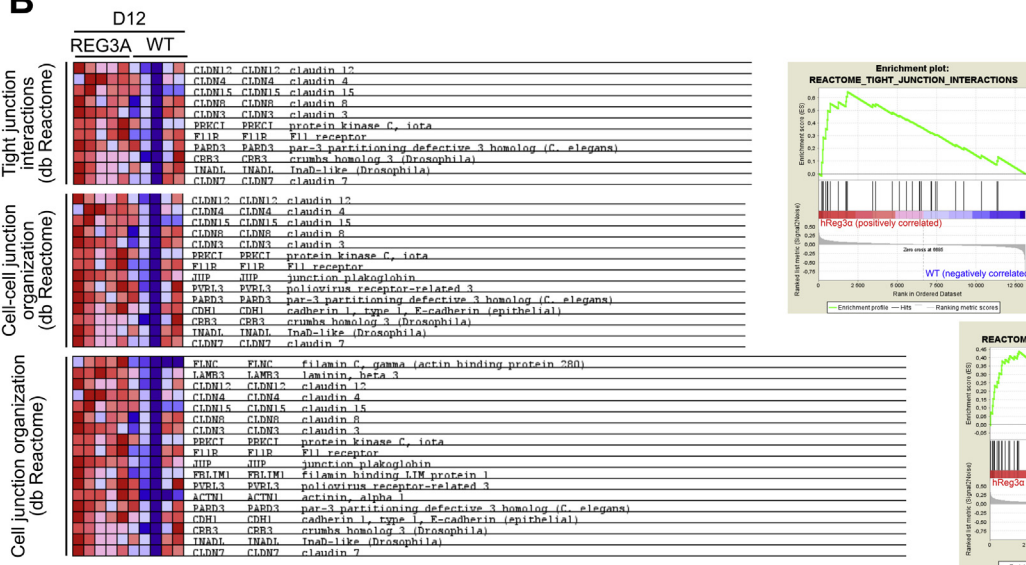


Supplementary Figure 6. Low susceptibility to induced colitis of *REG3A* heterozygous mice born to WT mothers compared with WT mice. (A–D) Time evolution of DSS-induced colitis in *REG3A* heterozygous (*REG3A-TG+/-*; n = 15), *REG3A* homozygous (*REG3A-TG+/+*; n = 12) and WT (n = 15) mice. (A) Body weight changes. (B) Rectal bleeding score. (C) Diarrhea score. (D) Kaplan-Meier survival plot. Heavy line: 5-day period of DSS administration. The data are means ± SEM. The Wilcoxon rank-sum test was performed for analysis. ***P* < .01, ****P* < .001.

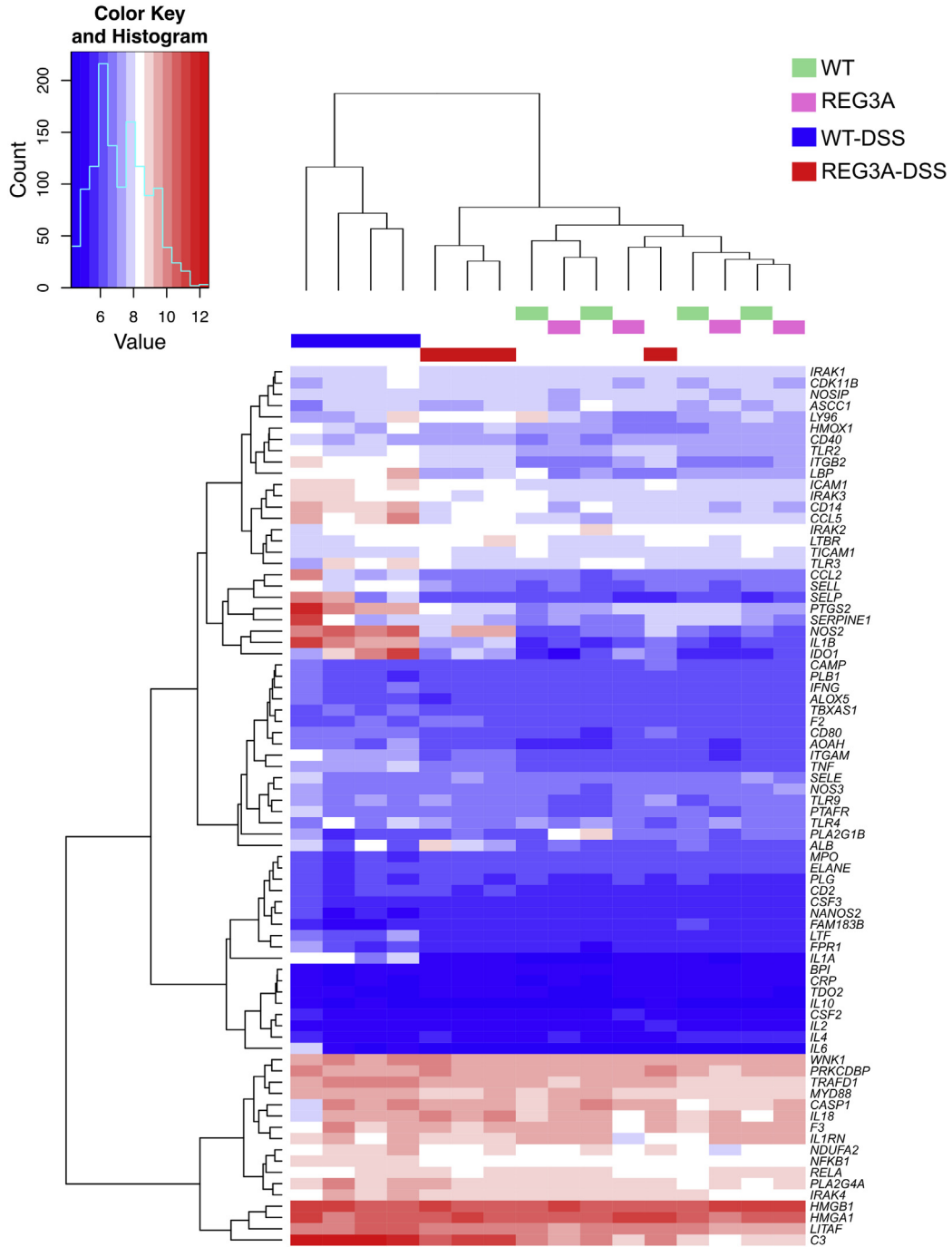
A



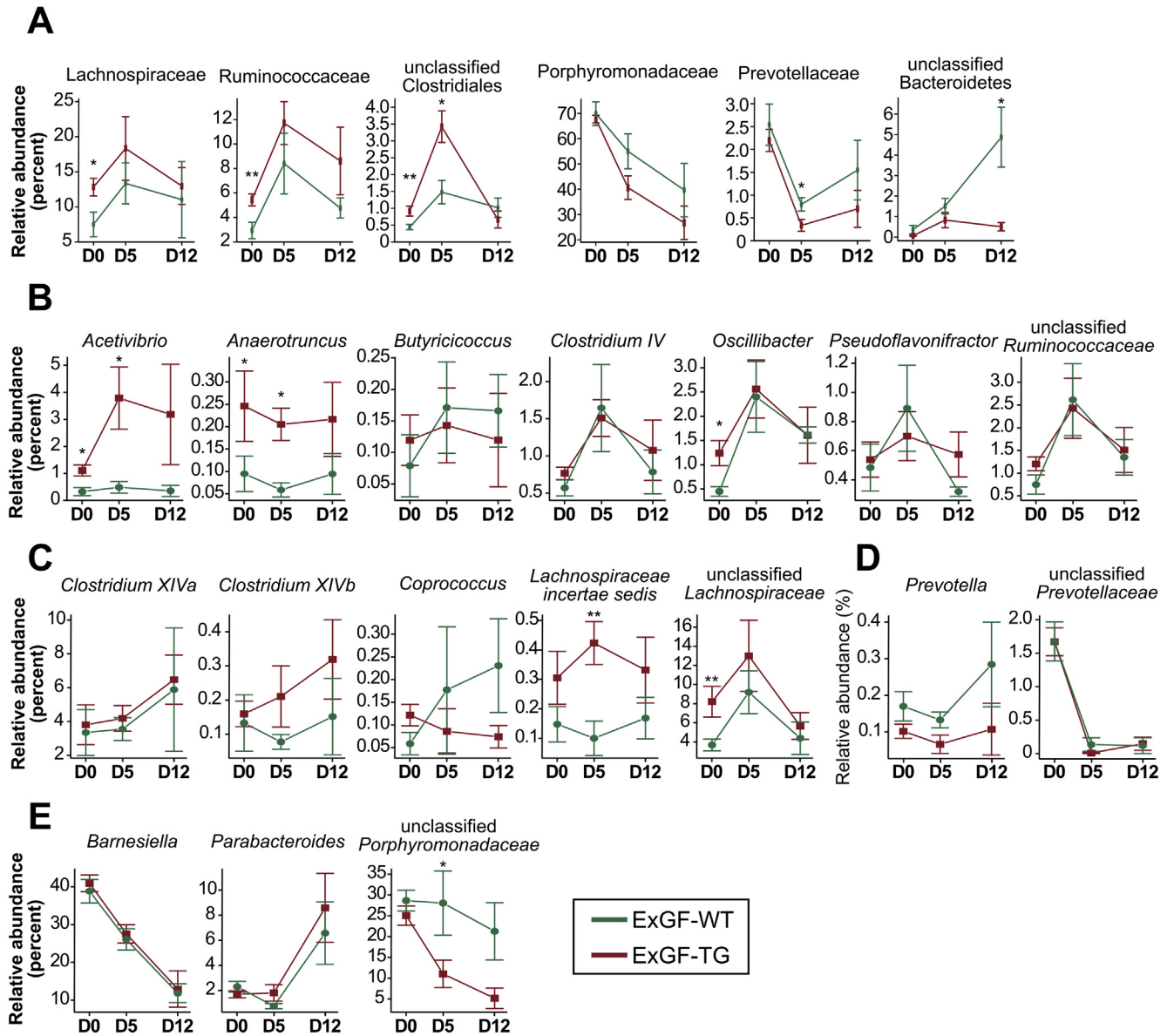
B



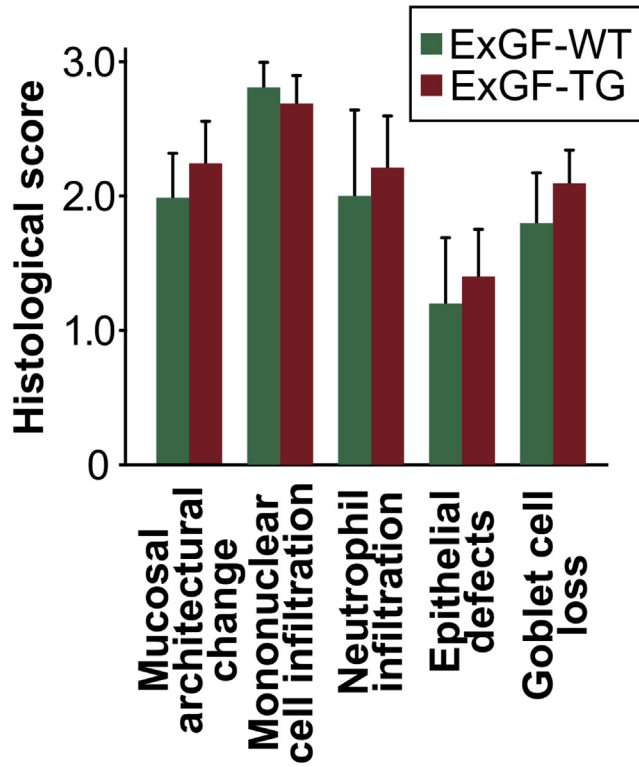
Supplementary Figure 7. Transcriptomic profiles of gene sets involved in the regulation of the gut barrier function. (A) and (B) Enrichment plots of genes related to gut barrier function and the corresponding heat maps for REG3A-TG and WT mice. (A) Homeostatic state (D0). (B) At day 12 of DSS-induced colitis (D12). $P < .001$ for all the indicated pathways (empirical phenotype-based permutation test).



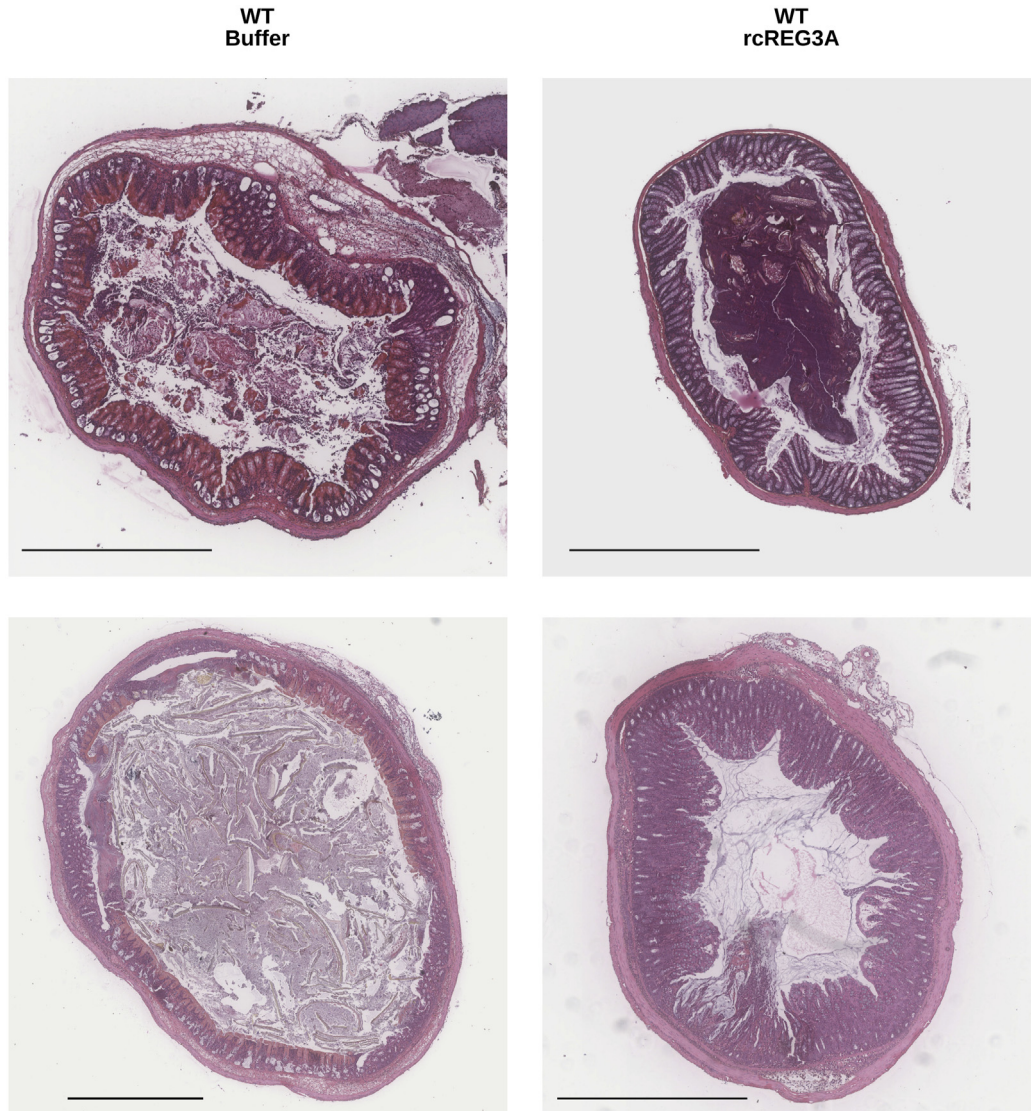
Supplementary Figure 8. Attenuation of the LPS activation pathway in the colon of *REG3A*-TG mice exposed to DSS. Hierarchical clustering for genes related to the LPS-induced activation pathway in healthy and DSS-given *REG3A*-transgenic and WT mice (n = 4 per group).



Supplementary Figure 9. Time evolution of bacterial communities in colonized germ-free mice during DSS-induced colitis. (A–E) Relative abundances of bacterial communities in germ-free mice colonized with the fecal microbiota from *REG3A*-TG (ExGF-TG; n = 8) and WT mice (ExGF-WT; n = 8) on days 0, 5, and 12 of DSS-induced colitis. (A) Bacterial families. (B–E) Bacterial genera of the following families: (B) Ruminococcaceae. (C) Lachnospiraceae. (D) Prevotellaceae. (E) Porphyromonadaceae. The data are means ± SEM. The 2-sided Wilcoxon rank-sum test was performed for analysis. **P* < .05, ***P* < .01.



Supplementary Figure 10. Gut barrier impairment in germ-free mice colonized with fecal microbiota from *REG3A*-transgenic (ExGF-TG; $n = 8$) and WT (ExGF-WT; $n = 8$) mice during DSS-induced colitis. Histological assessment of gut epithelium ($n = 8$ for each group). The data are means \pm SEM. $P =$ nonsignificant (Wilcoxon rank-sum test).



Supplementary Figure 11. Representative colon images from WT mice exposed to TNBS and administered 100 μ g of rcREG3A or an equivalent volume of buffer intrarectally. Staining: hematoxylin and eosin. Top row: full views of the same colon sections as in [Figure 6B](#). Scale bar, 1 mm.